

1-12-2016

A Bacterial Effector Co-opts Calmodulin to Target the Plant Microtubule Network

Ming Guo

University of Nebraska-Lincoln, mguo2@unl.edu

Panya Kim

University of Nebraska-Lincoln, pkim3@unl.edu

Guangyong Li

University of Nebraska-Lincoln, gli3@unl.edu


Christian Elowsky

University of Nebraska-Lincoln, celowsky@unl.edu

James R. Alfano

University of Nebraska-Lincoln, jalfano2@unl.edu

Follow this and additional works at: <https://digitalcommons.unl.edu/plantscifacpub>

 Part of the [Plant Biology Commons](#), [Plant Breeding and Genetics Commons](#), and the [Plant Pathology Commons](#)

Guo, Ming; Kim, Panya; Li, Guangyong; Elowsky, Christian; and Alfano, James R., "A Bacterial Effector Co-opts Calmodulin to Target the Plant Microtubule Network" (2016). *Faculty Publications from the Center for Plant Science Innovation*. 114.

<https://digitalcommons.unl.edu/plantscifacpub/114>

This Article is brought to you for free and open access by the Plant Science Innovation, Center for at DigitalCommons@University of Nebraska - Lincoln. It has been accepted for inclusion in Faculty Publications from the Center for Plant Science Innovation by an authorized administrator of DigitalCommons@University of Nebraska - Lincoln.

A Bacterial Effector Co-opts Calmodulin to Target the Plant Microtubule Network

Ming Guo,^{1,2} Panya Kim,^{1,3} Guangyong Li,^{1,2} Christian G. Elowsky,⁴ and James R. Alfano^{1,2}

1 Center for Plant Science Innovation, University of Nebraska–Lincoln, Lincoln, NE 68588-0660

2 Department of Plant Pathology, University of Nebraska–Lincoln, Lincoln, NE 68588-0722

3 School of Biological Sciences, University of Nebraska–Lincoln, Lincoln, NE 68588-0118

4 Center for Biotechnology, University of Nebraska–Lincoln, Lincoln, NE 68588-0665

Corresponding author — J.R. Alfano, jalfano2@unl.edu

Abstract

The bacterial pathogen *Pseudomonas syringae* depends on effector proteins secreted by its type III secretion system for the pathogenesis of plants. The majority of these effector proteins are known suppressors of immunity, but their plant targets remain elusive. Using *Arabidopsis thaliana* as a model host, we report that the HopE1 effector uses the host calcium sensor, calmodulin (CaM), as a co-factor to target the microtubule-associated protein 65 (MAP65), an important component of the microtubule network. HopE1 interacted with MAP65 in a CaM-dependent manner, resulting in MAP65-GFP dissociation from microtubules. Transgenic *Arabidopsis* expressing HopE1 had reduced secretion of the immunity protein PR-1 compared to wild-type plants. Additionally, *Arabidopsis map65-1* mutants were immune deficient and were more susceptible to *P. syringae*. Our results suggest a virulence strategy in which a pathogen effector is activated by host calmodulin to target MAP65 and the microtubule network, thereby inhibiting cell wall-based extracellular immunity.

Introduction

The Gram-negative bacterial pathogen *Pseudomonas syringae* can colonize the extracellular spaces between plant cells (i.e., the apoplast) of aerial plant tissue. *P. syringae* causes chlorotic lesions; however, because most *P. syringae* strains eventually cause some necrosis, they are generally designated as hemibiotrophs (Glazebrook, 2005). To grow in this niche and cause disease, *P. syringae* requires a type III protein secretion system, a molecular syringe that injects type III effector proteins into plant cells (Büttner, 2012). It now seems likely that most of these effectors suppress plant immunity, although the plant targets for the vast majority remain elusive (Block and Alfano, 2011; Dou and Zhou, 2012).

The plant immune system can be separated into two branches based on the microbial molecules that are recognized and the receptors that perceive them. The first branch uses extracellular pattern recognition receptors (PRRs) to recognize conserved microbial molecules known as pathogen-associated molecular patterns (PAMPs), which induce PAMP-triggered immunity (PTI; Zipfel, 2014). The second branch likely evolved after PTI and uses mostly intracellular nucleotide-binding/leucine-rich repeat (NLR) receptors historically known as resistance proteins, which recognize pathogen effectors inducing effector-triggered immunity (ETI; Cui et al., 2015). Both PTI and ETI induce a series of early immune responses such as reactive oxygen species (ROS) production, increase in intracellular calcium levels, phosphorylation events, gene expression, late immune responses such as callose (β -1,3-glucan) deposition in the cell wall, and secretion of pathogenesis-related (PR) proteins to the apoplast (Tsuda and Katagiri, 2010). The secretion of PR proteins to the apoplast is

part of the cell wall-based extracellular immunity employed by the plant to combat extracellular pathogens.

To be pathogenic, *P. syringae* must suppress or circumvent PTI and ETI. Failure to avoid either of these likely accounts for much of the host specificity of *P. syringae*. A primary strategy *P. syringae* uses to suppress PTI and ETI is to inject into plant cells type III effectors that target immunity components at seemingly every conceivable stage of plant immunity. These include PRRs and NLR receptor complexes, mitogen-activated protein kinase pathways, transcription, RNA translation, vesicle trafficking, phytohormone production, and the plant cytoskeleton (Block and Alfano, 2011). Through natural selection, type III effectors have evolved to target crucial components of immunity and therefore are important specialized tools to probe plant immunity.

The microtubule network plays essential roles in eukaryotes, including cell shape determination, cell division, and organelle transport (de Forges et al., 2012). Microtubules are made up of heterodimers of α/β -tubulin polymers forming nanotubule-like structures. They are nucleated at γ -tubulin complexes (Kollman et al., 2011) and exhibit dynamic instability—some regions are in a state of growth and others simultaneously in a state of shrinkage (Mitchison and Kirschner, 1984). Microtubule-associated proteins (MAPs), which include motor and non-motor proteins, help grow, break down, and rearrange microtubules to carry out specific cellular functions (Struk and Dhonukshe, 2014). One well-studied MAP is the MAP65/Ase1/PRC1 protein family, which is important for crosslinking anti-parallel microtubule bundles (Gaillard et al., 2008; Tulin et al., 2012). Relatively recently, the *P. syringae* type III effector HopZ1a was found to target tubulin (Lee et al., 2012), suggesting that the microtubule network is important for plant immunity.

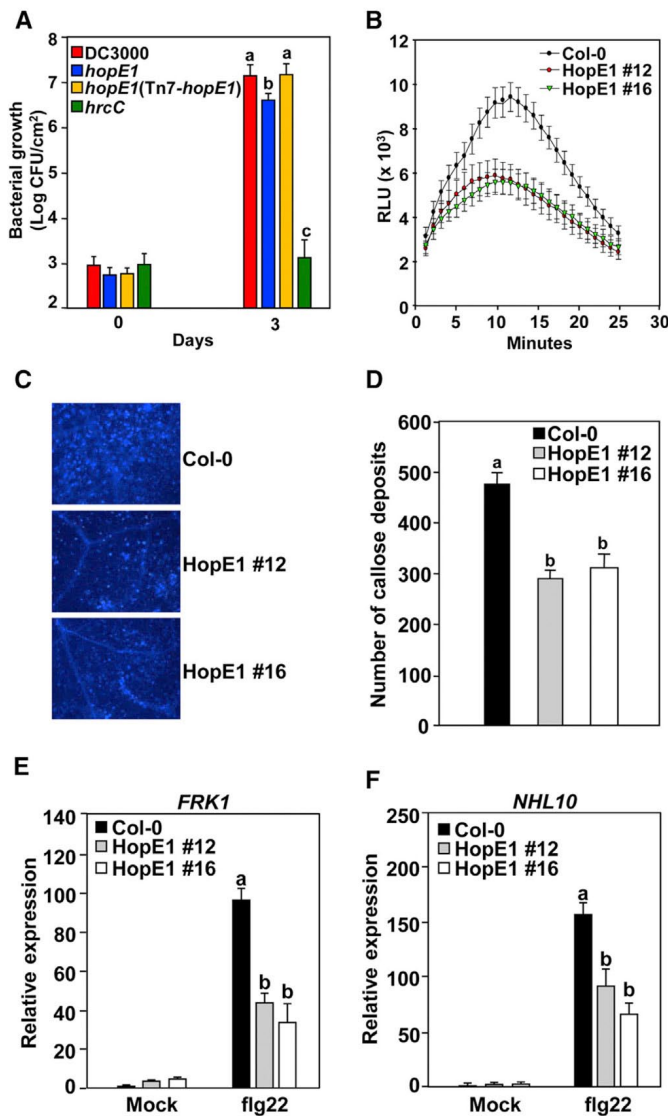


Figure 1. HopE1 Contributes to the Virulence of *P. syringae* and Suppresses PTI. (A) *Arabidopsis* plants were spray-inoculated with *P. syringae* pv. *tomato* (*Pto*) DC3000, a *Pto* DC3000 *hrcC* type III-defective mutant, a *Pto* DC3000 *hopE1* mutant, and a *hopE1*(Tn7-*hopE1*) complemented mutant. The experiments were repeated three times with similar results. Standard error bars are indicated. Different lowercase letters indicate statistical significance between treatments ($p < 0.01$). (B–F) *Arabidopsis* plants and two independent lines expressing HopE1-HA after treatment with flg22 (1 mM) were used in these experiments. (B) ROS production. Similar results were observed in four independent experiments. RLU, relative luminescence unit, $n = 24$. (C) Callose deposition. Leaf samples were stained with aniline blue, and callose deposits were visualized with fluorescence microscopy. (D) Quantification of callose deposits depicted in (C) using ImageJ. Values are means \pm SEM of 40 fields of view. Similar results were seen in three independent experiments. Different letters in the graph indicate statistical significance between treatments ($p < 0.01$). (E and F) Gene expression of two PTI-induced genes, *FRK1* (E) and *NHL10* (F). Gene expressions of *FRK1* and *NHL10* were analyzed with qRT-PCR. The relative expression levels were normalized to mock-treated *ACT2*. Values are presented as means \pm SEM. Experiments were repeated twice with similar results. See also Figure S1.

Here we report that the *P. syringae* pv. *tomato* (*Pto*) DC3000 effector HopE1 interacts with two *Arabidopsis* proteins—the calcium sensor calmodulin (CaM) and the microtubule-associated protein 65 (MAP65), a required component of the microtubule network. HopE1 dissociates MAP65-green fluorescent protein (GFP) from the microtubule network and inhibits secretion of an immunity-related protein. *Arabidopsis map65* mutants exhibit enhanced susceptibility to *P. syringae*, reduced PTI responses, and reduced secretion of an immunity-related protein, indicating that MAP65 is a component of plant immunity.

Results

HopE1 Suppresses Plant Immunity and Contributes to Virulence

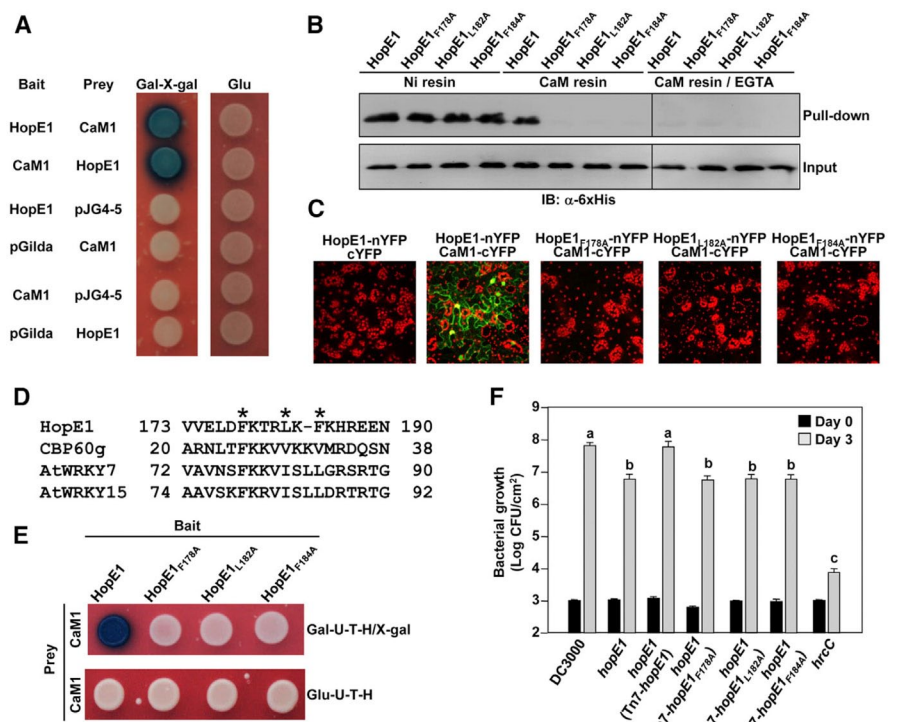
To evaluate HopE1's contribution to *P. syringae* virulence, we generated a *Pto* DC3000 *hopE1* mutant. The *Pto* DC3000 *hopE1* mutant was significantly reduced in its ability to grow in *Arabidopsis* leaf tissue compared to wild-type *Pto* DC3000 (Figure 1A). The weak reduction in in planta growth of single type III effector mutants is likely due to functional redundancy of type III effectors. Reintroduction of *hopE1* into the *Pto* DC3000 *hopE1* mutant restored in planta growth to wild-type *Pto* DC3000 levels (Figure 1A). Next we made transgenic *Arabidopsis* plants that expressed HopE1 fused to a hemagglutinin (HA) epitope after estradiol treatment (Figure S1A). *Arabidopsis* plants expressing HopE1-HA were reduced in both flg22 (a peptide derived from the flagellin PAMP)-induced ROS and callose deposition (Figures 1B–1D). Similar results were observed when elf18 (a peptide derived from the EF-Tu PAMP) and chitin were used to induce PTI in these plants (Figures S1B and S1C). Additionally, we also evaluated PTI-related gene expression after flg22 treatment and found that transgenic expression of HopE1-HA suppressed expression of two genes known to be induced by PTI (Figures 1E and 1F). Finally, to test if bacterially injected HopE1 exhibited the ability to suppress plant immunity, we used a non-pathogenic *P. fluorescens* (*Pf*) strain carrying pLN1965, a cosmid that encodes a functional *P. syringae* type III protein secretion system (Guo et al., 2009). Bacterially injected HopE1 also suppressed callose deposition, ROS production, and the expression of PTI-induced genes (Figures S1D–S1G). Collectively, these data indicate that HopE1 contributes to *P. syringae* virulence and suppresses multiple PTI responses.

HopE1 Interacts with Calmodulin

To better understand HopE1's role in virulence, we screened for proteins that interacted with HopE1 using a yeast two-hybrid (Y2H) system. Only seven different HopE1 interactors were identified from three independent Y2H screens (Figure 2A; Table S1). Six of these proteins were CaM isoforms, which function as calcium sensors in eukaryotes (Poovaiah et al., 2013), and the seventh interactor was microtubule-associated protein MAP65-1, a non-motor microtubule-associated protein that belongs to the MAP65/Ase1/PRC1 protein family (Walczak and Shaw, 2010).

To further validate the HopE1 and CaM interaction, we performed *in vitro* pull-down assays using CaM affinity resin. HopE1 fused to a six histidine tag (HopE1-His) was pulled down by the CaM resin (Figure 2B), indicating that HopE1-His interacts with CaM *in vitro*. The addition of the calcium chelator EGTA into the incubation mixture blocked the ability of CaM resin to pull down

Figure 2. HopE1 Interacts with Calmodulin (CaM), and Its CaM-Binding Site Is Required for Its Contribution to Virulence. (A) The interaction between HopE1 and Calmodulin 1 (CaM1) in a yeast two-hybrid assay. Yeast strains were grown on galactose (Gal) or glucose (Glu) media lacking uracil (U), tryptophan (T), and histidine (H). Gal-U-T-H medium contained bromo-4-chloro-3-indolyl- β -D-galactopyranoside (X-gal). Negative control strains contained the pGilda vector or the pJG4-5 vector. (B) In vitro pull-down of HopE1-His with CaM-affinity resin. Crude protein extracts from cultures of *E. coli* expressing HopE1-His, HopE1_{F178A}-His, HopE1_{L182A}-His, and HopE1_{F184A}-His were subjected to pull-down assays with CaM resin or Ni₂₊ resin. Eluted samples were subjected to immunoblot analysis using anti-His antibodies. The vertical lines in the Pull-down and Input images indicate where immunoblots were spliced together. (C) In vivo BiFC assays in *N. benthamiana*. HopE1 or HopE1 CaM-binding site mutants N-terminal (nYFP) fusions and CaM1 C-terminal (cYFP) fusions were expressed in *N. benthamiana* leaves using agroinfiltrations. Confocal images were taken 48 hr after infiltration. (D) An alignment of the putative CaM-binding site found in HopE1 with CaM-binding sites in representative *Arabidopsis* CaM-binding proteins. The asterisks indicate conserved hydrophobic amino acids that were mutated in HopE1 derivatives and used in experiments shown in this manuscript. (E) Yeast two-hybrid assays with CaM1 and HopE1 or HopE1 CaM-binding site mutants HopE1_{F178A}, HopE1_{L182A}, and HopE1_{F184A}. (F) Complementation of the *Pto* DC3000 *hopE1* mutant with HopE1 CaM-binding site mutation derivatives. The experiments were repeated three times with similar results. Standard error bars are indicated. Different letters indicate the statistical significance ($p < 0.05$). See also Figure S2



HopE1-His (Figure 2B), suggesting that the biologically active CaM form is required for CaM to interact with HopE1.

To determine if HopE1 interacts with CaM in planta, we performed bimolecular fluorescence complementation (BiFC) assays in *Nicotiana benthamiana* (Hu et al., 2002). We transiently co-expressed HopE1 fused with an N-terminal yellow fluorescence protein (YFP) fragment (HopE1-nYFP) with CaM1 fused with a C-terminal YFP fragment (CaM1-cYFP) in *N. benthamiana* leaves using *Agrobacterium*-mediated transformation (hereafter agroinfiltration), which resulted in bright YFP fluorescence visualized with confocal microscopy (Figures 2C and S2A). The BiFC fluorescence signal was localized to the cytoplasm and nucleus, similar to the localization observed for both HopE1-GFP and CaM1-GFP (Figure S2B).

HopE1's CaM-Binding Site in Its C Terminus Is Required for Its Contribution to Virulence and Immunity Suppression

We used BiFC assays with HopE1 derivatives to identify regions of HopE1 that bind to CaM. In these experiments we used agroinfiltration to transiently express HopE1 derivatives fused to nYFP with CaM1 fused to cYFP in *N. benthamiana*. We found that the HopE1-nYFP fusions that retained the ability to interact with CaM-cYFP all contained the C-terminal 52 amino acids of HopE1 (Figures S2C and S2D). Moreover, a HopE1-nYFP derivative that lacked amino acid residues 171–190 did not detectably interact with CaM-cYFP (Figures S2C and S2D). Interestingly, HopE1₁₇₁₋₁₉₀ is amphipathic (Figure S2E) and shares weak sequence similarity

to known CaM-binding sites of the *Arabidopsis* proteins CBP60g, WRKY7, and WRKY15 (Figure 2D) (Park et al., 2005; Wang et al., 2009). These data suggest that the CaM-binding site of HopE1 is within amino acid residues 171–190.

To determine if the putative CaM-binding site is required for the interaction between HopE1 and CaM1, Y2H constructs were made that encoded HopE1 derivatives containing single alanine substitutions in three different conserved hydrophobic amino acids in the putative CaM-binding site of HopE1. It has been demonstrated that analogous residues in other CaM-binding proteins are required to bind CaM (Park et al., 2005; Wang et al., 2009). All three HopE1 CaM-binding site mutants (HopE1_{F178A}, HopE1_{L182A}, and HopE1_{F184A}) displayed no detectable interaction with CaM1 in the Y2H system (Figure 2E). These *hopE1* mutant constructs made similar amounts of HopE1 derivatives in yeast, as did the construct encoding wild-type HopE1 (Figure S2F). We expressed these HopE1 derivatives in *E. coli*, and in contrast to wild-type HopE1, these were not pulled down by the CaM resin (Figure 2B). Furthermore, the peptide corresponding to the CaM-binding site of HopE1 can form stable complexes with CaM in the presence of calcium, but not EGTA (Figures S2G and S2H). Collectively, these data suggest that the CaM1-binding site of HopE1 resides within amino acids 171–190.

To determine whether the HopE1-CaM interaction is required for HopE1's contribution to *P. syringae* virulence, we complemented the *Pto* DC3000 *hopE1* mutant with the HopE1_{F178A}, HopE1_{L182A}, and HopE1_{F184A} derivatives that contained site-directed

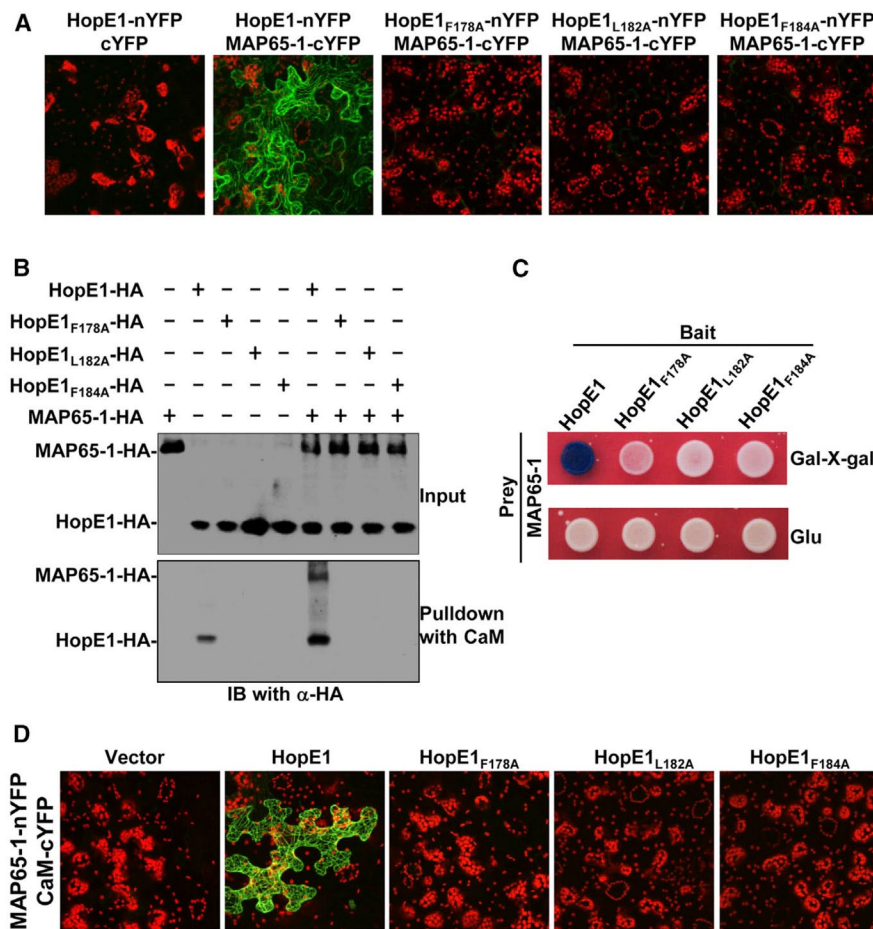


Figure 3. HopE1 Interacts CaM-Dependently with MAP65-1 (A) HopE1 and MAP65-1 interact in BiFC assays. HopE1-nYFP, HopE1_{F178A}-nYFP, HopE1_{L182A}-nYFP, and HopE1_{F184A}-nYFP with MAP65-1-cYFP or cYFP control were co-expressed in *N. benthamiana*. After 48 hr fluorescence was visualized with confocal microscopy. (B) Pull-down assays with CaM resin indicate that MAP65-1 interacts with CaM only in the presence of HopE1. Anti-HA antibodies were used for the immunoblot. (C) Yeast two-hybrid assays with CaM1 and HopE1 and HopE1 CaM-binding site mutants HopE1_{F178A}, HopE1_{L182A}, and HopE1_{F184A}. (D) MAP65-1 interacts with CaM in planta only in the presence of HopE1. In BiFC assays combinations of MAP65-1-nYFP and CaM1-cYFP in the presence of vector, HopE1-HA, HopE1_{F178A}-HA, HopE1_{L182A}-HA, or HopE1_{F184A}-HA were co-expressed in *N. benthamiana*. See also Figure S3.

mutations in HopE1's CaM-binding site. These HopE1 derivatives were unable to complement the reduced growth phenotype of the *Pto* DC3000 *hopE1* mutant (Figure 2F), suggesting that CaM is required for HopE1's contribution to virulence. Furthermore, these HopE1 CaM-binding site mutants fused to nYFP did not interact with CaM1-cYFP in BiFC assays (Figures 2C and S2A). Finally, we made *Arabidopsis* transgenic plants that separately expressed each HopE1 site-directed mutant (Figure S2I). These plants were unable to suppress flg22-induced callose or ROS production (Figures S2J and S2K), suggesting that CaM is required for HopE1 to suppress PTI.

HopE1 Binds to MAP65 in a CaM-Dependent Manner

We hypothesized that CaM may be either a true virulence target for HopE1 or a required co-factor. To further investigate HopE1 plant targets, we turned our attention to MAP65-1, the other *Arabidopsis* protein that interacted with HopE1 in our Y2H screens. We first performed BiFC assays in *N. benthamiana* to determine the extent to which these proteins interact in vivo. Using agroinfiltration, HopE1-nYFP and full-length MAP65-1 fused with cYFP (MAP65-1-cYFP) showed strong BiFC fluorescence that displayed a localization pattern typical of microtubule bundles (Figures 3A and S3A). To further examine this interaction, in vitro pull-down assays were performed using bacterially expressed HopE1 fused to a Flag tag (HopE1-Flag) and MAP65-1-His. Recombinant HopE1-Flag did not pull down MAP65-1-His in detectable amounts (Figure S3B), leading us to speculate that HopE1 requires CaM as a co-factor to interact with MAP65-1. To

test this, we performed pull-down experiments using CaM affinity resin to determine if recombinant MAP65-1 could be pulled down by CaM in the presence of HopE1-HA and found that CaM resin pulled down MAP65-1-HA only when HopE1-HA was present (Figure 3B). Next we tested whether the CaM-binding site of HopE1 is required for the HopE1-MAP65-1 interaction in these assays. The HopE1 CaM-binding site mutants HopE1_{F178A}, HopE1_{L182A}, and HopE1_{F184A} were unable to interact with MAP65-1 in BiFC, pull-down, and Y2H assays even though similar amounts of HopE1 were made (Figures 3A–3C and S3A–S3C). This finding suggests that CaM is required for the interaction between HopE1 and MAP65-1. To further test this idea, we performed BiFC assays between MAP65-1-nYFP and CaM-cYFP in the presence or absence of HopE1-HA or the HopE1-HA CaM-binding site mutants. YFP fluorescence in *N. benthamiana* was detectable only if wild-type HopE1 was present (Figures 3D and S3D). These data suggest that HopE1, CaM, and MAP65-1 form a complex inside plant cells.

Arabidopsis possesses nine members of the MAP65 family, which share 28%–79% similarity at the protein level (Hussey et al., 2002). MAP65 is broadly conserved in eukaryotes (Hussey et al., 2002), and the nine *Arabidopsis* MAP65 members fall in the same clade in a phylogenetic tree of the MAP65/Ase1/PRC1 family (Figure S3E). Of these, only MAP65-1, MAP65-2, MAP65-5, and MAP65-9 interacted with HopE1 in BiFC assays in *N. benthamiana* (Figures 3A and S3F). GFP fusions to all MAP65 homologs indicated that each localized to microtubules (Figure S3G).

HopE1 Dissociates MAP65-1 from the Microtubule Network

MAP65/Ase1/PRC1 family members crosslink microtubules, which is important for a functional microtubule network (Walczak and Shaw, 2010). To test our hypothesis that HopE1 targets MAP65 to perturb the microtubule network, we generated transgenic *Arabidopsis* plants that constitutively expressed MAP65-1-GFP and crossed these with the transgenic HopE1-HA plants described above. We isolated progeny that expressed both MAP65-1-GFP and HopE1-HA, the latter being produced after treatment with estradiol. We evaluated MAP65-1-GFP fluorescence with confocal microscopy at different time points after HopE1-HA induction. Fluorescence was almost completely absent 50 hr after estradiol treatment, indicating that HopE1 reduced the MAP65-1-GFP signal from microtubules (Figure 4A). Importantly, the reduced MAP65-1-GFP signal did not result from the degradation of MAP65-1-GFP protein, as the amount of MAP65-1-GFP was similar in the presence or absence of HopE1-HA (Figure 4B). Therefore, the diminished MAP65-1-GFP signal was most likely due to the redistribution of MAP65-1-GFP throughout the cytoplasm. We believe this to be the case because at high magnification MAP65-1-GFP is present in the cytoplasm in tissue expressing wild-type HopE1-HA (Figure S4A). Additionally, we quantified the fluorescence intensity in 30 different plant cells for each sample and found that MAP65-1-GFP fluorescence was greatly reduced after HopE1-HA induction (Figure 4C). We also made transgenic *Arabidopsis* plants expressing MAP65-1-GFP and the HopE1 CaM-binding site mutants. Co-expression of the HopE1-HA CaM-binding site mutants did not alter MAP65-1-GFP microtubule localization and did not significantly reduce the MAP65-1-GFP signal (Figures 4A–4C and S4A). To determine if HopE1 has a more general effect on the microtubule network, we crossed the transgenic HopE1-expressing plants with plants that expressed MAP4-GFP, TUB6-GFP, TUA6-GFP, or EB1-GFP, other proteins associated with the microtubule network (Marc et al., 1998; Mathur et al., 2003; Nakamura et al., 2004; Takemoto et al., 2003). In contrast to MAP65-1-GFP, HopE1-HA had no effect on the fluorescence signal emanating from these GFP fusions (Figures S4B–S4I). Therefore, these data suggest that HopE1 dissociates MAP65-1-GFP from the microtubule network and does not appear to have an effect on other microtubule-associated proteins or on the microtubule network itself.

Phenotypes observed in transgenic plants overexpressing a protein may not accurately represent the activity of the protein in more natural conditions. To determine whether HopE1 injected by the type III protein secretion system has effects similar to those observed in HopE1-HA-expressing transgenic *Arabidopsis* plants, we infiltrated different *Pto* DC3000 strains into *Arabidopsis* plants expressing MAP65-1-GFP and evaluated the MAP65-1-GFP signal at different time intervals after infection. While the reduction in the GFP signal was not as robust as observed in transgenic HopE1-HA plants, the presence of HopE1 in *Pto* DC3000 strains with a functional type III protein secretion system caused a reduction of the MAP65-1-GFP signal (Figures 4D and 4E). Importantly, plants infiltrated with the *Pto* DC3000 *hopE1* mutant did exhibit greater MAP65-1-GFP fluorescence compared to strains that produced HopE1 (Figures 4D and 4E). Wild-type HopE1-HA complemented the *Pto* DC3000 *hopE1* mutant; however, the HopE1 CaM-binding site mutants did not (Figures 4D and 4E). The plants infected with the different bacterial

strains produced similar amounts of MAP65-1-GFP throughout the time course (Figure S4J). The increased fluorescence in MAP65-1-GFP in plants infiltrated with the *Pto* DC3000 *hrcC* mutant compared to the *Pto* DC3000 *hopE1* mutant suggests that other type III effectors in this strain may target the microtubule network (Figures 4D and 4E).

To evaluate HopE1's effect on MAP65-1-GFP in the absence of other effectors, we again used the non-pathogenic *Pf*(pLN1965). MAP65-1-GFP plants were infiltrated with the *Pf*(pLN1965) strain with and without a plasmid construct encoding HopE1-HA. Significant decreases of MAP65-1-GFP fluorescence was observed in plants infiltrated with *Pf*(pLN1965)(*phopE1-HA*) compared to *Pf*(pLN1965) with a vector control (Figures S4K and S4L). Collectively, these results suggest that transgenically expressed or bacterially delivered HopE1 dissociates MAP65-1-GFP from the microtubule network.

HopE1 Inhibits Plant Protein Secretion

The microtubule network is involved in many processes in eukaryotes, including protein secretion (Boutté et al., 2007; Crowell et al., 2009). Because *P. syringae* is an extracellular pathogen present in the plant apoplast, we speculated that HopE1 may target MAP65 to inhibit protein secretion and cell wall-based extracellular immunity. To test if HopE1 inhibits protein secretion, we used two established protein secretion assays. The first utilized a GFP derivative (secGFP) fused at its N terminus to a secretion signal peptide from the immunity-related *Arabidopsis* protein PR-3 (Batoko et al., 2000; Haseloff et al., 1997; Zheng et al., 2004). In this assay, the secGFP fluorescence is stronger if secGFP remains cell-bound and diminishes upon its secretion to the extracellular milieu. Using agroinfiltrations, the secGFP reporter was transiently expressed in *N. benthamiana* alone, with HopE1-HA, or with one of the HopE1-HA CaM-binding site mutants. As shown in Figure 5A, the secGFP fluorescence was greater when HopE1 was present, even though the amount of secGFP present was similar in all leaf tissue samples (Figure 5B), indicating that wild-type HopE1 inhibits the secretion of secGFP. Inclusion of the HopE1-HA CaM-binding site mutants suggests that CaM is required for the inhibition of secGFP secretion by HopE1 (Figures 5A and 5B).

To substantiate this observation, we investigated the extent to which HopE1 inhibited the secretion of a specific immunity-related protein in plants. PR proteins such as PR-1, which are rapidly induced and accumulate in plants attacked by pathogens, play important roles in plant immunity (van Loon et al., 2006). PR-1 has been shown to be secreted to the apoplast as part of the immune response, and it has been used as a reporter for immunity-related secretion when plants are induced with SA or its analogs (Kalde et al., 2007; Wang et al., 2005). Strikingly, PR-1 levels were greatly reduced in extracellular fluid isolated from HopE1-expressing plants treated with SA compared to wild-type *Arabidopsis* (Figures 5C and S5A). Wild-type levels of PR-1 were found in the extracellular fluid of *Arabidopsis* plants expressing HopE1 derivatives containing mutations in their CaM-binding sites (Figure 5C), suggesting that CaM is needed for the inhibition of PR-1 secretion. To test whether bacterially injected HopE1 also inhibited PR-1 secretion, we again used the non-pathogenic *Pf*(pLN1965) with a vector control, a construct encoding wild-type HopE1, or a construct encoding a HopE1 CaM-binding site mutant. PR-1 secretion was reduced only in the strain that also

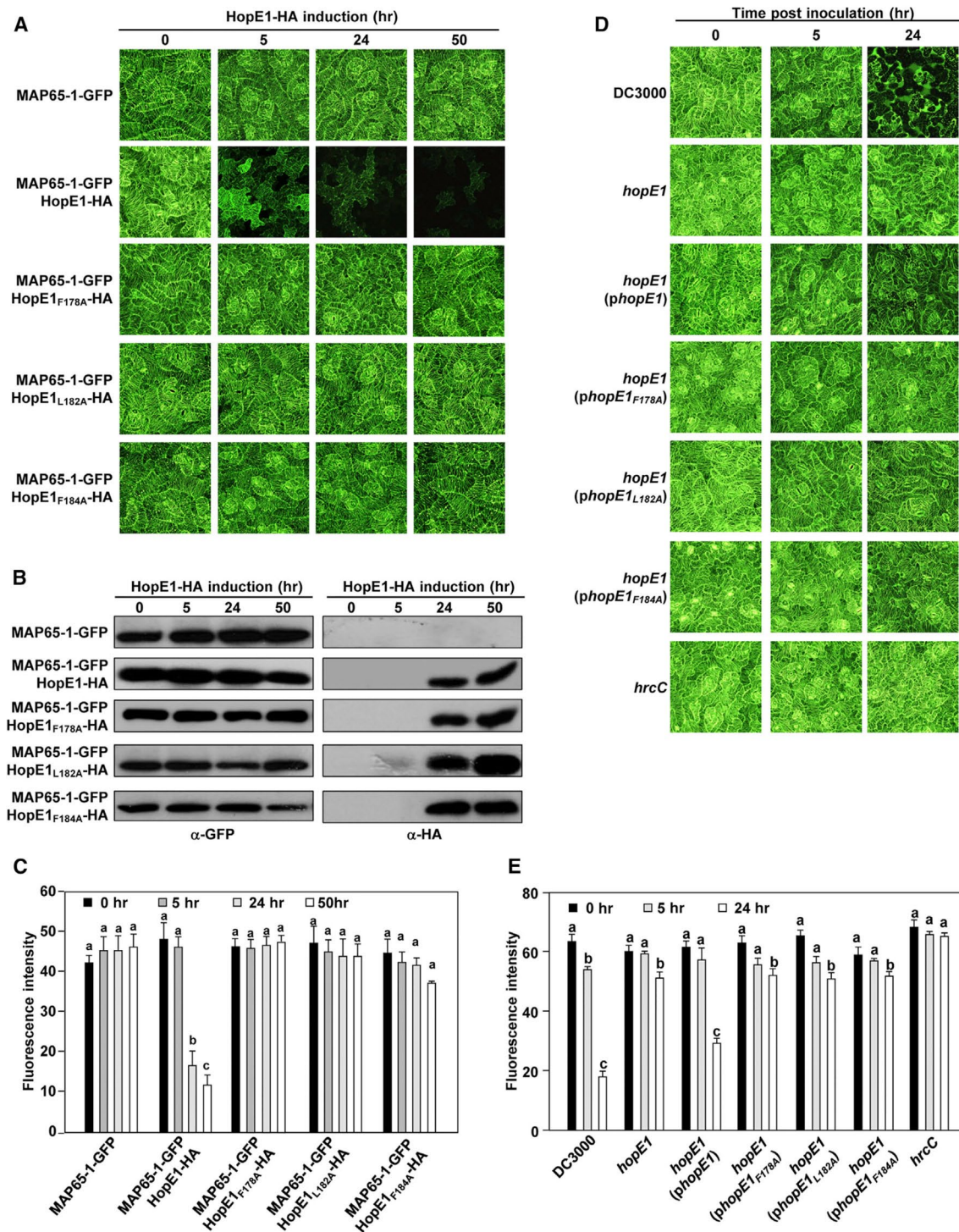


Figure 4. HopE1 Dissociates MAP65-1 from Microtubules (A) *Arabidopsis* plants expressing MAP65-1-GFP alone or with HopE1-HA, HopE1_{F178A}-HA, HopE1_{L182A}-HA, or HopE1_{F184A}-HA were treated with 20 mM estradiol. MAP65-1-GFP fluorescence was monitored with confocal microscopy at the indicated time points (hr, hours) after estradiol treatment. (B) Immunoblot analysis of MAP65-1-GFP and HopE1-HA, HopE1_{F178A}-HA, HopE1_{L182A}-HA, and HopE1_{F184A}-HA from plants in (A). (C) Quantification of fluorescence intensity of MAP65-1-GFP from plants used in (A). Different lowercase letters indicate statistical significance between time points ($p < 0.05$). The values are means \pm SEM, $n = 30$. (D) *Arabidopsis* MAP65-1-GFP transgenic plants were syringe-infiltrated with the following bacterial strains at 10^7 cells/ml: *Pto* DC3000, *Pto* DC3000 *hopE1* mutant, *Pto* DC3000 *hopE1*(*phopE1*), *hopE1*(*phopE1*_{F178A}), *hopE1*(*phopE1*_{L182A}), *hopE1*(*phopE1*_{F184A}), and a type III-defective mutant *hrcC*. MAP65-1-GFP signals were monitored with confocal microscopy at the indicated time points (hr, hours) after infiltration. (E) Quantification of fluorescence intensity of MAP65-1-GFP from plants used in (D). Different lowercase letters indicate statistical significance between time points ($p < 0.05$). The values are means \pm SEM, $n = 30$. See also Figure S4.

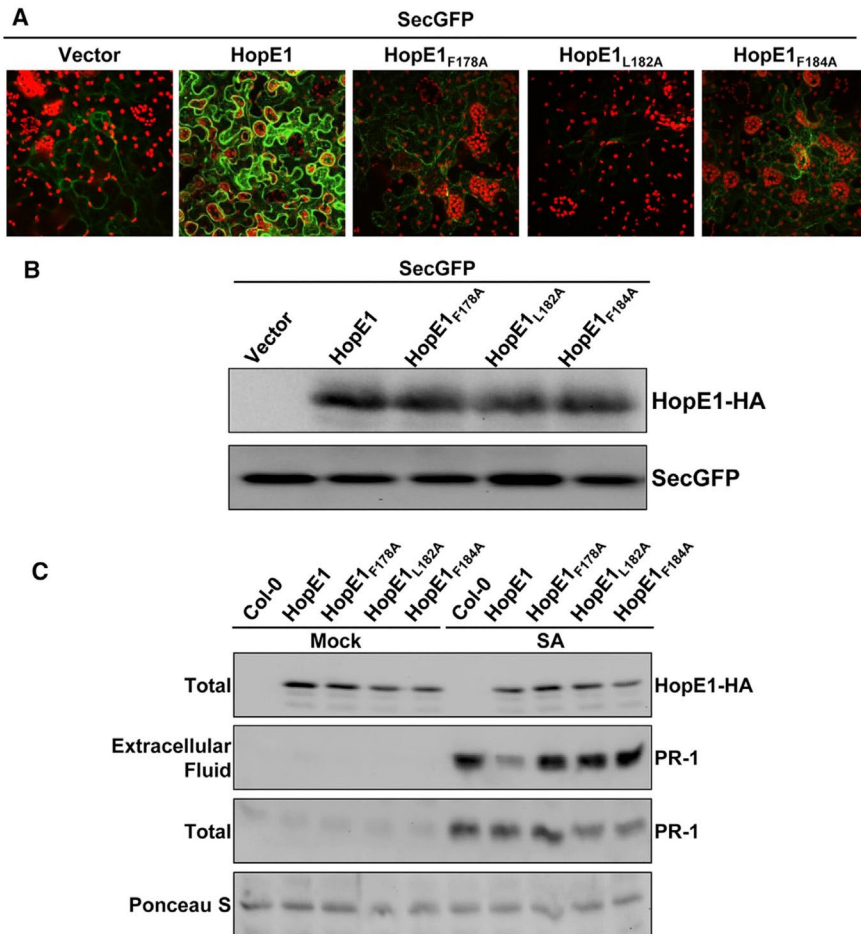


Figure 5. HopE1 Interferes with Protein Secretion in Plants (A) GFP with a PR-3 secretion signal (SecGFP) was co-expressed with HopE1-HA, HopE1_{F178A}-HA, HopE1_{L182A}-HA, HopE1_{F184A}-HA, or the vector control via agroinfiltrations in *N. benthamiana*. Confocal images were captured 48 hr after coinfiltration. (B) Immunoblot analysis with anti-GFP antibodies or anti-HA antibodies of protein samples of the plant tissue shown in (A). (C) Leaf extracellular fluid was isolated after mock or salicylic acid (SA) treatment and analyzed with immunoblots. A Ponceau S-stained membrane is shown to evaluate protein loading. See also Figure S5.

expressed wild-type HopE1-HA (Figure S5B). Together these results suggest that HopE1 inhibits the secretion of PR-1 in a CaM-dependent manner.

Arabidopsis map65 Mutants Exhibit Enhanced Disease Susceptibility to *P. syringae* and Reduced PR-1 Secretion

To assess whether MAP65 proteins are involved in plant immunity to bacteria, we determined if *map65* mutants were altered in PTI and susceptibility to *P. syringae*. We focused on MAP65-1 and MAP65-2 because MAP65-1 was identified in our Y2H screen and MAP65-2 is its closest homolog (Figure S3E) (Hussey et al., 2002). We obtained the *Arabidopsis* mutants *map65-1* and *map65-2*, and a *map65-1 map65-2* double mutant (Lucas et al., 2011). These plant mutants, along with wild-type *Arabidopsis*, were spray-inoculated with wild-type *Pto* DC3000. *Arabidopsis map65-1* and the double mutant exhibited enhanced susceptibility based on increased growth of *Pto* DC3000 3 days after inoculation, as well as enhanced disease symptom production (Figures 6A and 6B). The *map65-2* mutant was not significantly different from wild-type *Arabidopsis* in susceptibility to *P. syringae*. Interestingly, when the *Pto* DC3000 *hopE1* mutant was spray-inoculated into the *Arabidopsis map65-1* and the *map65-1 map65-2* mutants, it no longer displayed a reduced growth phenotype (Figure 6C), suggesting that MAP65-1 is a primary target of HopE1.

We further evaluated these mutants for defects in plant immunity by quantifying ROS production and callose deposition

after treatment with flg22. The *map65-1* and *map65-1 map65-2* plants were greatly reduced in ROS and callose compared to wild-type *Arabidopsis* (Figures 6D and 6E). ROS production in the *map65-2* mutant was slightly reduced compared with wild-type *Arabidopsis*, even though it was similar to wild-type plants in *P. syringae* susceptibility (Figures 6A and 6B) and callose deposition (Figure 6E). Thus, MAP65-2 may contribute subtly to immunity, and the ROS assay was perhaps sensitive enough to detect this contribution. We evaluated the gene expression of the *Arabidopsis* MAP65 gene family in leaf tissue and found that MAP65-1 and MAP65-4, and to a lesser extent MAP65-5, were induced by SA, suggesting that these MAP65 homologs may be more involved in plant immunity than the other family members (Figure S6). Next we evaluated *map65-1*, *map65-2*, and *map65-1 map65-2* mutant plants for PR-1 secretion. The *map65-1* and *map65-1 map65-2* plants, but not *map65-2*, showed reduced secretion of PR-1 to the extracellular milieu (Figure 6F). Together these results indicate that MAP65-1 plays an important role in protein secretion and plant immunity.

Discussion

We show here that HopE1 makes a substantial contribution to virulence, and, in addition to suppressing ETI (Guo et al., 2009; Jamir et al., 2004), it suppresses PTI (Figure 1), although the molecular mechanism by which it does is unknown. It does not

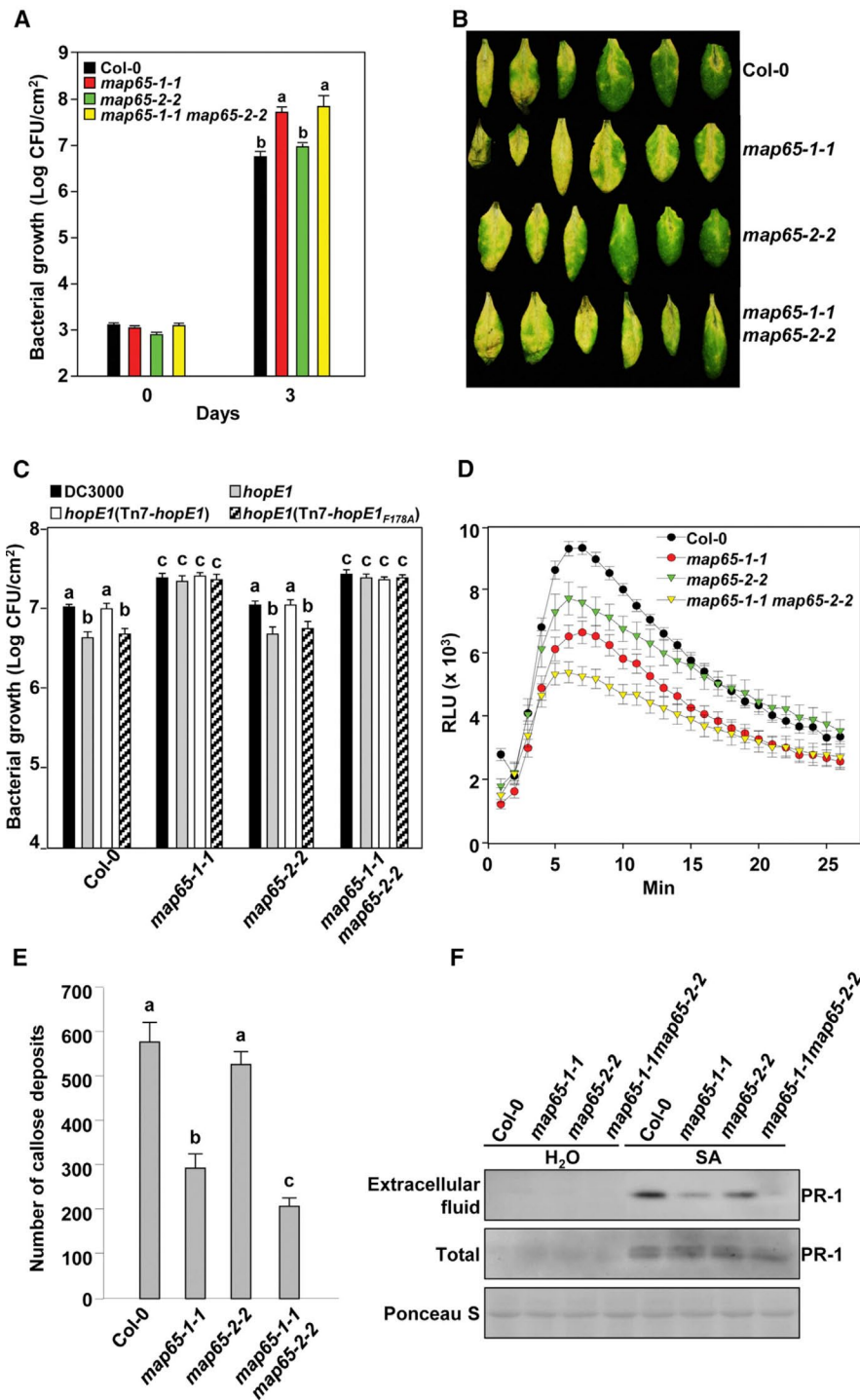


Figure 6. MAP65 Is a Component of Plant Immunity (A) The growth of *Pto* DC3000 in *Arabidopsis* (Col-0) and *map65* mutants. The experiments were repeated three times with similar results. Standard error bars are indicated. Different letters indicate the statistical significance ($p < 0.05$). (B) Disease symptom production in the plants used in (A). Pictures were taken 5 days after inoculation with *Pto* DC3000. (C) The growth of *Pto* DC3000 and *hopE1* mutant strains in wild-type *Arabidopsis* (Col-0) and the *map65* mutants. The bacterial growth of the indicated strains 3 days after inoculation is shown. The bacterial numbers of the strains at day 0 were not significantly different. The experiments were repeated twice with similar results. Values are means \pm SEM, $n = 4$. Different letters indicate the statistical significance ($p < 0.05$). (D) Leaf disks were treated with flg22 (1 mM) and ROS production was determined. This experiment was done three times with similar results. Standard error bars are indicated ($n = 12$). RLU, relative luminescence unit. (E) Callose deposition in *Arabidopsis map65* mutants. The values are means \pm SEM, $n = 40$. Statistical significance ($p < 0.05$) is indicated with different letters. (F) PR-1 secretion in *Arabidopsis map65* mutants. Samples were subjected to immunoblot analysis with anti-PR-1 antibodies. A Ponceau S-stained membrane indicates equal loading. See also Figure S6.

appear to function by destabilizing its target, as do several other *P. syringae* type III effectors (Jiang et al., 2013; Nomura et al., 2006; Shao et al., 2003), because MAP65-1 is stable in the presence of HopE1 (Figure 4B). However, the fact that it suppresses both ETI and PTI suggests that it is acting on a component of plant immunity used in both immunity types or that it targets distinct components in each. Our finding that HopE1 targets MAP65-1 and the microtubule network is consistent with HopE1 suppressing both PTI and ETI because the microtubule network is likely important for both types of immunity.

MAP65/Ase1/PRC1 family members are non-motor microtubule-associated proteins that play important roles in microtubules by cross-linking them in antiparallel arrays (Gaillard et al., 2008; Janson et al., 2007; Tulin et al., 2012). Together with the kinesin motor proteins (Cross and McInish, 2014), which can cross-link and move microtubules relative to one another, they control the properties of microtubules. Mutants lacking MAP65/Ase1/PRC1 family members have defects in microtubule cross-linking and function (Loiodice et al., 2005; Yamashita et al., 2005). Plants have multiple MAP65/Ase1/PRC1 family members, unlike

other eukaryotes that generally have only one. It is likely multiple MAP65 homologs are present in plants because microtubules play additional roles in plants compared to in other eukaryotes. Our results suggest that MAP65-1, and perhaps other MAP65 homologs, play roles in *Arabidopsis* immunity, most likely in their involvement in the secretion of immunity-related products to the apoplast at sites of pathogen ingress.

The cell cortex of plants is associated with interphase microtubules, called cortical microtubules, near the plasma membrane (Ehrhardt and Shaw, 2006), in contrast to the cell cortex of mammalian cells, which is mainly associated with actin (Pesen and Hoh, 2005). Cortical microtubules are required for cell and tissue morphogenesis and are associated with the targeted exocytosis of cell wall components (Lloyd, 2011). We show here that at least one MAP65 homolog is targeted by HopE1, that HopE1 can disrupt the secretion of secGFP (which contains the secretion signal from PR-3) and the immunity-related protein PR-1 (Figure 5), and that *Arabidopsis map65-1* mutants exhibit increased susceptibility to *P. syringae*, reduced immune responses, and reduced PR-1 secretion (Figure 6). These results suggest that cortical microtubules play an important role in the secretion of immunity-related products to the apoplast, perhaps by recruiting factors important for secretion.

However, it should be noted that the microtubule network was not dramatically altered in plants expressing HopE1-HA (Figures S4B–S4I) other than the dissociation of MAP65-1 from microtubules. Consistent with this is the fact that the *Arabidopsis map65-1 map65-2* double mutant has a wild-type-like microtubule network (Lucas et al., 2011). Thus, our hypothesis is that HopE1 subtly affects the microtubule network by targeting MAP65-1 and possibly other MAP65 homologs such that it dampens plant immunity, likely through the inhibition of protein secretion.

How might HopE1 disrupt MAP65 function? Our results suggest that HopE1 can dissociate MAP65-1-GFP from microtubules (Figure 4). Because MAP65 homologs have a microtubule-binding domain in their C termini (Smertenko et al., 2008), the simplest scenario is that HopE1 directly or indirectly modifies MAP65 so its microtubule-binding domain can no longer associate with microtubules. Phosphorylation of the C-terminal region in *Arabidopsis* and tobacco MAP65 homologs has been shown to reduce their ability to cross-link microtubules (Sasabe and Machida, 2006; Smertenko et al., 2006); therefore, HopE1 or the CaM/HopE1/MAP65 complex may directly or indirectly induce phosphorylation or another enzymatic modification of MAP65 to dissociate it from microtubules. Future studies will determine if HopE1 can modify MAP65 to perturb its function in the microtubule network. Additionally, because the *Pto* DC3000 *hrcC* mutant exhibited increased MAP65-1-GFP fluorescence compared to the *Pto* DC3000 *hopE1* mutant (Figure 4E), other type III effectors also may target MAP65 and/or microtubules; therefore, we will evaluate the ability of other *Pto* DC3000 type III effectors to target the microtubule network.

We found that the calcium sensor CaM is required for HopE1 to interact with MAP65 (Figure 3) and therefore acts as a co-factor for HopE1. No other plant pathogen effector has been shown to use CaM as a co-factor. Indeed, the only mammalian pathogen effectors known to use CaM as a co-factor are the *Bordetella pertussis* CyaA toxin (Wolff et al., 1980) and the *Bacillus anthracis* Anthrax edema factor toxin (Leppa, 1982), both nontype

III adenylate cyclases. The fact that these adenylate cyclases co-opt CaM as a co-factor may not be that surprising since several mammalian adenylate cyclases also use CaM as a cofactor (Monneron et al., 1988). It seems likely that HopE1 acquired the use of CaM from plants since CaM is found only in eukaryotes. Because some plant MAPs use CaM as a co-factor, the genes encoding these represent a potential source for the CaM-binding site present in HopE1 (Bürstenbinder et al., 2013).

There are at least three possible reasons a requirement for calcium and CaM evolved for HopE1's activation. First, because calcium levels increase when plant immunity is triggered (Poovaiah et al., 2013), linking HopE1 activation to calcium/CaM may be a way to ensure that HopE1 is not active inside host cells unless it has perceived the presence of a pathogen. Second, the CaM requirement may be a way to ensure that HopE1 would be a later-acting effector. There are examples of temporal regulation of *Salmonella* effectors inside mammalian cells (Kubori and Galán, 2003). Third, using CaM as a cofactor may be an evolutionary strategy to ensure that HopE1 is active only in host cells. Several *P. syringae* type III effectors have been shown to use cofactors that are present only in eukaryotic cells (Coaker et al., 2005; Giska et al., 2013; Lee et al., 2012; Li et al., 2013).

The plant immunity activation process begins with pathogen perception triggering signal transduction pathways, followed by transcriptional reprogramming, production of immunity-related products, and the delivery of these products to the apoplast, where *P. syringae* actually resides in the host. The underpinning mechanisms that deliver these products and the specific products important for resistance to bacterial pathogens remain largely unknown. Our finding that HopE1 co-opts CaM to target MAP65 and the microtubule network highlights the importance of the secretion of immunity-related products, cell wall-based extracellular immunity, and the apoplastic environment for the bacterial pathogenicity of plants.

Experimental Procedures

Bacterial Strains, Constructs, and Primers

The strains and constructs used in this study are listed in Table S2, and the primers used are listed in Table S3.

Construction of *P. syringae* DC3000 *hopE1* Mutants

A modified unmarked mutagenesis strategy (House et al., 2004) was used to construct *Pto* DC3000 *hopE1* mutants. Also see Supplemental Experimental Procedures.

Plant Materials

Following standard methods, transgenic *A. thaliana* Col-0 plants were generated by floral-dipping transformation with *A. tumefaciens*. Also see Supplemental Experimental Procedures.

In Planta Bacterial Growth Assay

Plant pathogenicity assays were done as previously described (Block et al., 2014). Also see Supplemental Experimental Procedures.

Agrobacterium-Mediated Transient Assays

Agrobacterium strains carrying binary constructs were infiltrated into *N. benthamiana* leaves at an OD₆₀₀ of 0.8. Samples were harvested 48 hr after infiltration for either immunoblot analyses or imaging of fluorescence proteins using confocal microscopy.

Yeast Two-Hybrid Assay

PCR-amplified genes or desired DNA regions were cloned into

either the bait vector pGILDA or the prey vector pJG4-5. The resulting pGilda and pJG4-5 constructs were transformed into yeast strain EGY48(pSH18-34). To evaluate the activity of the *lacZ* reporter, the interactions were examined on galactose-Ura-His-Trp dropout medium containing X-gal (5-bromo-4-chloro-3-indolyl- β -D-galactopyranoside). For cDNA library screening, *hopE1* was cloned into pGilda, resulting in pLN504, which was transformed into the yeast strain EGY48(pSH18-34). The resulting yeast strain EGY48(pSH18-34)(pLN504) was transformed with an *Arabidopsis* cDNA library in pJG4-5 (Mackey et al., 2002). The interactors were screened based on their growth on galactose-Ura-His-Trp-Leu dropout medium.

BiFC Assay

For BiFC constructs, the appropriate DNAs were PCR-amplified with specific primer sets containing engineered 3' restriction sites, along with the DNA regions corresponding to nYFP (1–155 amino acids) or cYFP (156–243 amino acids), including their stop codons and an introduced 50 restriction site. The gene-specific PCR products were digested with restriction enzymes and ligated with either nYFP or cYFP. PCR products digested with the same restriction enzymes and the ligated products served as templates in PCR reactions. The fused DNA fragments were cloned into pENTR, and the resulting constructs were recombined with the binary destination construct pLN462 by LR reactions. The resulting plasmids were transformed into *Agrobacterium* C58C1. *Agrobacterium* strains carrying nYFP or cYFP fusion constructs were co-infiltrated into *N. benthamiana* leaves. The interaction was determined 48 hr after infiltration based on YFP fluorescence.

ROS Production Assay

ROS production was determined following a previously described protocol (Asai and Yoshioka, 2008). The intensity of ROS generation was determined by counting photons from L-012-mediated luminescence monitored with a Synergy 5 luminometer (BioTek).

Callose Deposition Assay

Callose deposition assays were done as previously described (Adam and Somerville, 1996). Also see Supplemental Experimental Procedures.

Quantitative RT-PCR Analyses

RNA was extracted with RNeasy miniprep kit (QIAGEN) following manufacturer's instructions. cDNAs were synthesized using iScript reverse transcriptase- supermix for RT-PCR (Bio-Rad). qRT-PCR was performed using iTaq universal SYBR Green supermix (Bio-Rad) with a Bio-Rad CFX Connect Real-Time System. *ACTIN2* was used as a reference gene for normalization of gene expression. The relative gene expression was determined by calculating with $2^{-\Delta\Delta CT}$, and the normalized transcript levels were compared to wild-type Col-0.

Immunoblot Analyses

After separation with SDS-PAGE, proteins were blotted on PVDF membranes with a semi-wet transfer. Standard protocols were followed for immunoblots. The following primary antibodies were purchased from commercial suppliers: anti-Flag, Sigma; anti-HA, Roche; anti-His, Invitrogen; anti-LexA, Pierce Antibodies; anti-PR-1, AgriSera; and anti-GFP, Abcam. All secondary antibodies conjugated with alkaline phosphatase were purchased from Sigma.

CaM Affinity Resin Pull-Downs

CaM affinity resins were purchased from Agilent Technologies. CaM pull-down assays were done by following manufacturer's instructions. Also see Supplemental Experimental Procedures.

Quantification of GFP Fluorescence Intensity

The GFP fluorescence intensity was quantified with ImageJ. The fluorescence was quantified from three fields of view for each sample. In each, ten plant cells were used for quantification. Also see Supplemental Experimental Procedures.

SecGFP Assay

SecGFP assay was carried out with *Agrobacterium*-mediated transient expression in *N. benthamiana*. Briefly, an *Agrobacterium* strain carrying pVKHEn6-secGFP at an OD₆₀₀ of 0.01 was co-infiltrated with another *Agrobacterium* strain carrying pER8::*hopE1*-HA, pER8::*hopE1*_{F178A}-HA, pER8::*hopE1*_{L182A}-HA, pER8::*hopE1*_{F184A}-HA, or a vector control in *N. benthamiana* leaves (Batoko et al., 2000; Zheng et al., 2004). Estradiol (20 μ M) was sprayed 24 hr after infiltration to induce HopE1-HA expression. Confocal images were taken 48 hr after infiltration.

Analysis of Secreted Protein in Extracellular Fluids

Extracellular fluids were extracted as previously described with modification (Speth et al., 2009). Briefly, *Arabidopsis* plants were treated with SA at 100 mM or, for mock control, H₂O. Estradiol (20 mM) was sprayed onto HopE1-HA, HopE1_{F178A}-HA, HopE1_{L182A}-HA, and HopE1_{F184A}-HA transgenic plants 24 hr prior to the SA treatment to induce the expression of HopE1-HA. Twenty-four hours after SA treatment, the treated and control plant leaves were detached and vacuum infiltrated for 1 min with PBS (pH 7.4) containing 0.002% Silwet L-77 (Lehle Seeds). The vacuum-infiltrated leaves were put in poly-prep columns (Bio-Rad) placed in 50 ml conical centrifuge tubes (Nalgene). Extracellular fluids were collected by centrifugation at 5003 *g* for 10 min at 4° C. The volume of extracellular fluids was measured with a micropipette, and an appropriate volume of loading buffer was added. The samples were subjected to SDS-PAGE and immunoblot analyses with anti-PR-1 antibodies.

Supplemental Information

Supplemental Information includes Supplemental Experimental Procedures, six figures, and three tables and can be found with this article online at <http://dx.doi.org/10.1016/j.chom.2015.12.007>.

Author Contributions

M.G., P.K., G.L., and C.G.E. performed the experiments; M.G., P.K., G.L., C.G.E., and J.R.A. designed the experiments; M.G. and J.R.A. wrote the manuscript. All authors commented on the manuscript.

Acknowledgments — We thank members of the Alfano laboratory for fruitful discussions on the experiments described in this paper and E. Banset for editing. We thank Drs. J. Dangl for the *Arabidopsis* yeast two-hybrid cDNA library; S. Shaw for *Arabidopsis* *map65-1*, *map65-2*, and *map65-1 map65-2* mutants; H. Jin and X. Dong for anti-PR-1 antibodies; D. Desveaux for *Arabidopsis* MAP4-GFP and EB1-GFP seed; and S. Ro-batzek for *Arabidopsis* MAP4-GFP, TUA6-GFP, and TUB6-GFP seed. This research was supported by a University of Nebraska internal grant and a grant from the Nebraska Soybean Board.

References

- Adam, L., and Somerville, S.C. (1996). Genetic characterization of five powdery mildew disease resistance loci in *Arabidopsis thaliana*. *Plant J.* 9, 341–356.
- Asai, S., and Yoshioka, H. (2008). The role of radical burst via MAPK signaling in plant immunity. *Plant Signal. Behav.* 3, 920–922.
- Batoko, H., Zheng, H.Q., Hawes, C., and Moore, I. (2000). A rab1 GT-Pase is required for transport between the endoplasmic reticulum and golgi apparatus and for normal golgi movement in plants. *Plant Cell* 12, 2201–2218.
- Block, A., and Alfano, J.R. (2011). Plant targets for *Pseudomonas syringae* type III effectors: virulence targets or guarded decoys? *Curr. Opin. Microbiol.* 14, 39–46.
- Block, A., Toruño, T.Y., Elowsky, C.G., Zhang, C., Steinbrenner, J., Beynon, J., and Alfano, J.R. (2014). The *Pseudomonas syringae* type III effector HopD1 suppresses effector-triggered immunity, localizes to the endoplasmic reticulum, and targets the *Arabidopsis* transcription factor NTL9. *New Phytol.* 201, 1358–1370.

- Boutté, Y., Vernhettes, S., and Siaty-Jeunemaitre, B. (2007). Involvement of the cytoskeleton in the secretory pathway and plasma membrane organisation of higher plant cells. *Cell Biol. Int.* *31*, 649–654.
- Bürstenbinder, K., Savchenko, T., Müller, J., Adamson, A.W., Stamm, G., Kwong, R., Zipp, B.J., Dinesh, D.C., and Abel, S. (2013). *Arabidopsis* calmodulin-binding protein IQ67-domain 1 localizes to microtubules and interacts with kinesin light chain-related protein-1. *J. Biol. Chem.* *288*, 1871–1882.
- Büttner, D. (2012). Protein export according to schedule: architecture, assembly, and regulation of type III secretion systems from plant- and animal-pathogenic bacteria. *Microbiol. Mol. Biol. Rev.* *76*, 262–310.
- Coaker, G., Falick, A., and Staskawicz, B. (2005). Activation of a phytopathogenic bacterial effector protein by a eukaryotic cyclophilin. *Science* *308*, 548–550.
- Cross, R.A., and McAinsh, A. (2014). Prime movers: the mechanochemistry of mitotic kinesins. *Nat. Rev. Mol. Cell Biol.* *15*, 257–271.
- Crowell, E.F., Bischoff, V., Desprez, T., Rolland, A., Stierhof, Y.D., Schumacher, K., Gonneau, M., Höfte, H., and Vernhettes, S. (2009). Pausing of Golgi bodies on microtubules regulates secretion of cellulose synthase complexes in *Arabidopsis*. *Plant Cell* *21*, 1141–1154.
- Cui, H., Tsuda, K., and Parker, J.E. (2015). Effector-triggered immunity: from pathogen perception to robust defense. *Annu. Rev. Plant Biol.* *66*, 487–511.
- de Forges, H., Bouissou, A., and Perez, F. (2012). Interplay between microtubule dynamics and intracellular organization. *Int. J. Biochem. Cell Biol.* *44*, 266–274.
- Dou, D., and Zhou, J.M. (2012). Phytopathogen effectors subverting host immunity: different foes, similar battleground. *Cell Host Microbe* *12*, 484–495.
- Ehrhardt, D.W., and Shaw, S.L. (2006). Microtubule dynamics and organization in the plant cortical array. *Annu. Rev. Plant Biol.* *57*, 859–875.
- Gaillard, J., Neumann, E., Van Damme, D., Stoppin-Mellet, V., Ebel, C., Barbier, E., Geelen, D., and Vantard, M. (2008). Two microtubule-associated proteins of *Arabidopsis* MAP65s promote antiparallel microtubule bundling. *Mol. Biol. Cell* *19*, 4534–4544.
- Giska, F., Lichočka, M., Piechocki, M., Dadlez, M., Schmelzer, E., Hennig, J., and Krzymowska, M. (2013). Phosphorylation of HopQ1, a type III effector from *Pseudomonas syringae*, creates a binding site for host 14-3-3 proteins. *Plant Physiol.* *161*, 2049–2061.
- Glazebrook, J. (2005). Contrasting mechanisms of defense against biotrophic and necrotrophic pathogens. *Annu. Rev. Phytopathol.* *43*, 205–227.
- Guo, M., Tian, F., Wamboldt, Y., and Alfano, J.R. (2009). The majority of the type III effector inventory of *Pseudomonas syringae* pv. *tomato* DC3000 can suppress plant immunity. *Mol. Plant Microbe Interact.* *22*, 1069–1080.
- Haseloff, J., Siemering, K.R., Prasher, D.C., and Hodge, S. (1997). Removal of a cryptic intron and subcellular localization of green fluorescent protein are required to mark transgenic *Arabidopsis* plants brightly. *Proc. Natl. Acad. Sci. USA* *94*, 2122–2127.
- House, B.L., Mortimer, M.W., and Kahn, M.L. (2004). New recombination methods for *Sinorhizobium meliloti* genetics. *Appl. Environ. Microbiol.* *70*, 2806–2815.
- Hu, C.D., Chinenov, Y., and Kerppola, T.K. (2002). Visualization of interactions among bZIP and Rel family proteins in living cells using bimolecular fluorescence complementation. *Mol. Cell* *9*, 789–798.
- Hussey, P.J., Hawkins, T.J., Igarashi, H., Kaloriti, D., and Smertenko, A. (2002). The plant cytoskeleton: recent advances in the study of the plant microtubule-associated proteins MAP-65, MAP-190 and the *Xenopus* MAP215-like protein, MOR1. *Plant Mol. Biol.* *50*, 915–924.
- Jamir, Y., Guo, M., Oh, H.-S., Petnicki-Ocwieja, T., Chen, S., Tang, X., Dickman, M.B., Collmer, A., and Alfano, J.R. (2004). Identification of *Pseudomonas syringae* type III effectors that can suppress programmed cell death in plants and yeast. *Plant J.* *37*, 554–565.
- Janson, M.E., Loughlin, R., Loïdouce, I., Fu, C., Brunner, D., Né dé lec, F.J., and Tran, P.T. (2007). Crosslinkers and motors organize dynamic microtubules to form stable bipolar arrays in fission yeast. *Cell* *128*, 357–368.
- Jiang, S., Yao, J., Ma, K.W., Zhou, H., Song, J., He, S.Y., and Ma, W. (2013). Bacterial effector activates jasmonate signaling by directly targeting JAZ transcriptional repressors. *PLoS Pathog.* *9*, e1003715.
- Kalde, M., Nühse, T.S., Findlay, K., and Peck, S.C. (2007). The syntaxin SYP132 contributes to plant resistance against bacteria and secretion of pathogenesis-related protein 1. *Proc. Natl. Acad. Sci. USA* *104*, 11850–11855.
- Kollman, J.M., Merdes, A., Mourey, L., and Agard, D.A. (2011). Microtubule nucleation by γ -tubulin complexes. *Nat. Rev. Mol. Cell Biol.* *12*, 709–721.
- Kubori, T., and Galán, J.E. (2003). Temporal regulation of *Salmonella* virulence effector function by proteasome-dependent protein degradation. *Cell* *115*, 333–342.
- Lee, A.H., Hurley, B., Felsensteiner, C., Yea, C., Ckurshumova, W., Bartetzko, V., Wang, P.W., Quach, V., Lewis, J.D., Liu, Y.C., et al. (2012). A bacterial acetyltransferase destroys plant microtubule networks and blocks secretion. *PLoS Pathog.* *8*, e1002523.
- Leppla, S.H. (1982). Anthrax toxin edema factor: a bacterial adenylate cyclase that increases cyclic AMP concentrations of eukaryotic cells. *Proc. Natl. Acad. Sci. USA* *79*, 3162–3166.
- Li, W., Yadeta, K.A., Elmore, J.M., and Coaker, G. (2013). The *Pseudomonas syringae* effector HopQ1 promotes bacterial virulence and interacts with tomato 14-3-3 proteins in a phosphorylation-dependent manner. *Plant Physiol.* *161*, 2062–2074.
- Lloyd, C. (2011). Dynamic microtubules and the texture of plant cell walls. *Int. Rev. Cell Mol. Biol.* *287*, 287–329.
- Loïdouce, I., Staub, J., Setty, T.G., Nguyen, N.P., Paoletti, A., and Tran, P.T. (2005). Ase1p organizes antiparallel microtubule arrays during interphase and mitosis in fission yeast. *Mol. Biol. Cell* *16*, 1756–1768.
- Lucas, J.R., Courtney, S., Hassfurder, M., Dhingra, S., Bryant, A., and Shaw, S.L. (2011). Microtubule-associated proteins MAP65-1 and MAP65-2 positively regulate axial cell growth in etiolated *Arabidopsis* hypocotyls. *Plant Cell* *23*, 1889–1903.
- Mackey, D., Holt, B.F., 3rd, Wiig, A., and Dangl, J.L. (2002). RIN4 interacts with *Pseudomonas syringae* type III effector molecules and is required for RPM1-mediated resistance in *Arabidopsis*. *Cell* *108*, 743–754.
- Marc, J., Granger, C.L., Brincat, J., Fisher, D.D., Kao, Th., McCubbin, A.G., and Cyr, R.J. (1998). A GFP-MAP4 reporter gene for visualizing cortical microtubule rearrangements in living epidermal cells. *Plant Cell* *10*, 1927–1940.
- Mathur, J., Mathur, N., Kernebeck, B., Srinivas, B.P., and Hülskamp, M. (2003). A novel localization pattern for an EB1-like protein links microtubule dynamics to endomembrane organization. *Curr. Biol.* *13*, 1991–1997.

- Mitchison, T., and Kirschner, M. (1984). Dynamic instability of microtubule growth. *Nature* 312, 237–242.
- Monneron, A., Ladant, D., d'Alayer, J., Bellalou, J., Ba[^] rzu, O., and Ullmann, A. (1988). Immunological relatedness between *Bordetella pertussis* and rat brain adenylyl cyclases. *Biochemistry* 27, 536–539.
- Nakamura, M., Naoi, K., Shoji, T., and Hashimoto, T. (2004). Low concentrations of propyzamide and oryzalin alter microtubule dynamics in *Arabidopsis* epidermal cells. *Plant Cell Physiol.* 45, 1330–1334.
- Nomura, K., Debroy, S., Lee, Y.H., Pumplin, N., Jones, J., and He, S.Y. (2006). A bacterial virulence protein suppresses host innate immunity to cause plant disease. *Science* 313, 220–223.
- Park, C.Y., Lee, J.H., Yoo, J.H., Moon, B.C., Choi, M.S., Kang, Y.H., Lee, S.M., Kim, H.S., Kang, K.Y., Chung, W.S., et al. (2005). WRKY group IId transcription factors interact with calmodulin. *FEBS Lett.* 579, 1545–1550.
- Pesen, D., and Hoh, J.H. (2005). Micromechanical architecture of the endothelial cell cortex. *Biophys. J.* 88, 670–679.
- Poovaliah, B.W., Du, L., Wang, H., and Yang, T. (2013). Recent advances in calcium/calmodulin-mediated signaling with an emphasis on plant-microbe interactions. *Plant Physiol.* 163, 531–542.
- Sasabe, M., and Machida, Y. (2006). MAP65: a bridge linking a MAP kinase to microtubule turnover. *Curr. Opin. Plant Biol.* 9, 563–570.
- Shao, F., Golstein, C., Ade, J., Stoutemyer, M., Dixon, J.E., and Innes, R.W. (2003). Cleavage of *Arabidopsis* PBS1 by a bacterial type III effector. *Science* 301, 1230–1233.
- Smertenko, A.P., Chang, H.Y., Sonobe, S., Fenyk, S.I., Weingartner, M., Bögre, L., and Hussey, P.J. (2006). Control of the AtMAP65-1 interaction with microtubules through the cell cycle. *J. Cell Sci.* 119, 3227–3237.
- Smertenko, A.P., Kaloriti, D., Chang, H.Y., Fiserova, J., Opatrny, Z., and Hussey, P.J. (2008). The C-terminal variable region specifies the dynamic properties of *Arabidopsis* microtubule-associated protein MAP65 isoforms. *Plant Cell* 20, 3346–3358.
- Speth, E.B., Imboden, L., Hauck, P., and He, S.Y. (2009). Subcellular localization and functional analysis of the *Arabidopsis* GTPase RabE. *Plant Physiol.* 149, 1824–1837.
- Struk, S., and Dhonukshe, P. (2014). MAPs: cellular navigators for microtubule array orientations in *Arabidopsis*. *Plant Cell Rep.* 33, 1–21.
- Takemoto, D., Jones, D.A., and Hardham, A.R. (2003). GFP-tagging of cell components reveals the dynamics of subcellular re-organization in response to infection of *Arabidopsis* by oomycete pathogens. *Plant J.* 33, 775–792.
- Tsuda, K., and Katagiri, F. (2010). Comparing signaling mechanisms engaged in pattern-triggered and effector-triggered immunity. *Curr. Opin. Plant Biol.* 13, 459–465.
- Tulin, A., McClerklin, S., Huang, Y., and Dixit, R. (2012). Single-molecule analysis of the microtubule cross-linking protein MAP65-1 reveals a molecular mechanism for contact-angle-dependent microtubule bundling. *Biophys. J.* 102, 802–809.
- van Loon, L.C., Rep, M., and Pieterse, C.M. (2006). Significance of inducible defense-related proteins in infected plants. *Annu. Rev. Phytopathol.* 44, 135–162.
- Walczak, C.E., and Shaw, S.L. (2010). A MAP for bundling microtubules. *Cell* 142, 364–367.
- Wang, D., Weaver, N.D., Kesarwani, M., and Dong, X. (2005). Induction of protein secretory pathway is required for systemic acquired resistance. *Science* 308, 1036–1040.
- Wang, L., Tsuda, K., Sato, M., Cohen, J.D., Katagiri, F., and Glazebrook, J. (2009). *Arabidopsis* CaM binding protein CBP60g contributes to MAMP-induced SA accumulation and is involved in disease resistance against *Pseudomonas syringae*. *PLoS Pathog.* 5, e1000301.
- Wolff, J., Cook, G.H., Goldhammer, A.R., and Berkowitz, S.A. (1980). Calmodulin activates prokaryotic adenylate cyclase. *Proc. Natl. Acad. Sci. USA* 77, 3841–3844.
- Yamashita, A., Sato, M., Fujita, A., Yamamoto, M., and Toda, T. (2005). The roles of fission yeast ase1 in mitotic cell division, meiotic nuclear oscillation, and cytokinesis checkpoint signaling. *Mol. Biol. Cell* 16, 1378–1395.
- Zheng, H., Kunst, L., Hawes, C., and Moore, I. (2004). A GFP-based assay reveals a role for RHD3 in transport between the endoplasmic reticulum and Golgi apparatus. *Plant J.* 37, 398–414.
- Zipfel, C. (2014). Plant pattern-recognition receptors. *Trends Immunol.* 35, 345–351.

Supplemental Information

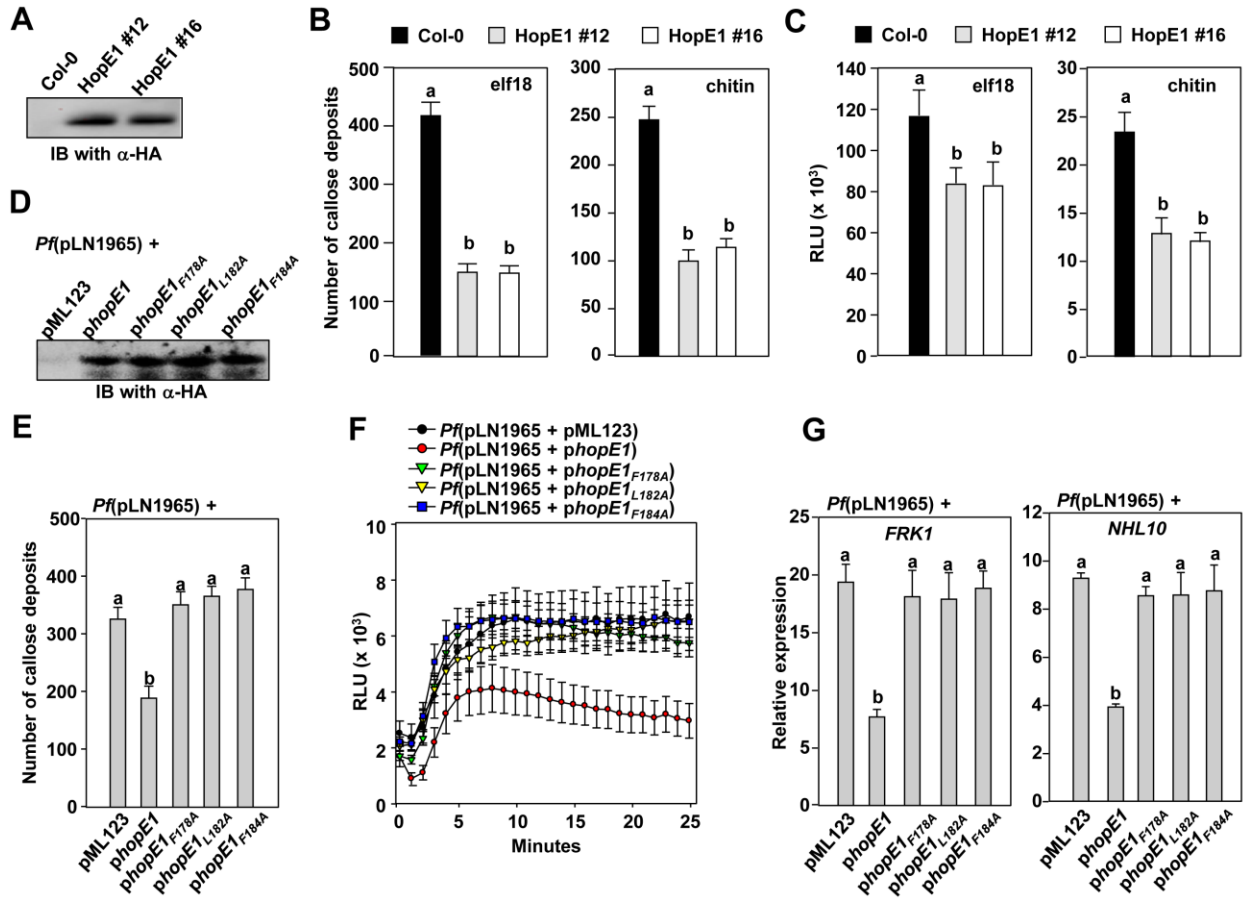


Figure S1. Additional Evidence that HopE1 suppresses PTI, Related to Figure 1. (A) Immunoblot analysis of transgenic Arabidopsis lines that express HopE1-HA. Arabidopsis plants were treated with estradiol (20 μ M) and after 24 hours plant tissue was harvested and subjected to immunoblot analysis with anti-HA antibodies. These plants were used in experiments described in Figs. 1B-F and S1B-C. (B-C) Experiments used Arabidopsis plants and transgenic lines (#12 & #16) of Arabidopsis expressing HopE1-HA. Plants were treated with elf18 (1 μ M) or chitin (100 μ g/ml). (B) Callose deposition in Arabidopsis (Col-0) and lines (#12 & #16) expressing HopE1-HA. The values are means \pm SEM, n=40. Different lowercase letters in the graphs indicate statistical significance between treatments (P<0.01). Three independent experiments showed similar results. (C) ROS production in Arabidopsis (Col-0) and lines (#12 & #16) expressing HopE1-HA. Similar results were observed in four independent experiments. RLU, relative luminescence unit, n=24. The values are means \pm SEM. (D) Immunoblots of *Pseudomonas fluorescens*(pLN1965) strains carrying pML123, *phopE1*, *phopE1*_{F178A}, *phopE1*_{L182A}, or *phopE1*_{F184A}. (E) Callose deposition in Arabidopsis plants infiltrated with the bacterial strains listed in (D). The values are means \pm SEM, n=20. (F) ROS production in Arabidopsis plants infiltrated with the bacterial strains listed in (D). (G) Expression of two PTI-induced genes, *FRK1* and *NHL10* was determined in wild type Arabidopsis. Plants were infiltrated with the bacterial strains listed in (D) and gene expression of *FRK1* and *NHL10* was analyzed with qRT-PCR. The relative expression levels were normalized to mock-treated *ACT2*. Values are presented as means \pm SEM. Experiments were repeated twice with similar results.

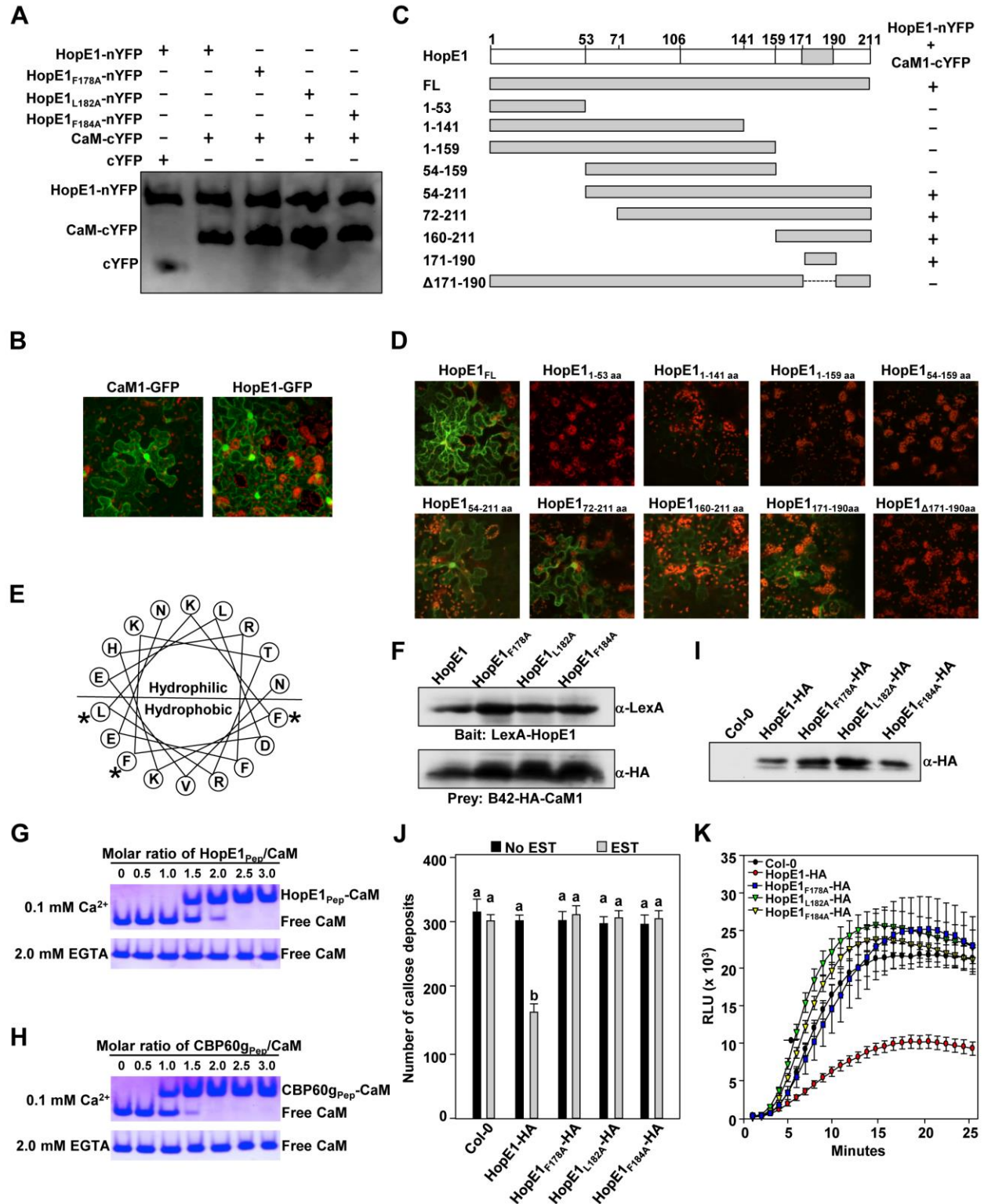


Figure S2. Delimiting HopE1's CaM-binding Site, Related to Figure 2. (A) Immunoblots showing expression of constructs used in BiFC assay in Fig. 2C. (B) Localization of HopE1-GFP and CaM1-GFP in *N. benthamiana*. (C) A schematic representation of the HopE1-nYFP truncations used to identify regions of HopE1 that interact with CaM1-cYFP. Full-length (FL) HopE1-nYFP and HopE1-nYFP truncations were used in BiFC assays with CaM-

cYFP. A '+' score indicates a visible YFP signal and a '-' indicates no visible signal. **(D)** Interactions of HopE1-nYFP derivatives depicted in (C) with CaM1-cYFP in BiFC assays. **(E)** A helical wheel representation of the HopE1₁₇₁₋₁₉₀ truncation showing the amphipathicity of HopE1's putative CaM-binding site. The asterisks indicate conserved hydrophobic amino acids that were mutated in HopE1 derivatives used in several experiments described in this paper. **(F)** Immunoblots of crude samples of the yeast strains used in yeast two-hybrid assays shown in Fig. 2E. **(G-H)** Gel mobility shift assay of HopE1's CaM-binding site with CaM. Peptides corresponding to the CaM-binding site of HopE1 (HopE1_{Pep}; **G**) and the CaM-binding site of Arabidopsis CBP60g (CBP60g_{Pep}; **H**) were incubated with bovine CaM in the presence of 0.1 mM CaCl₂ (upper panels) or 2.0 mM EGTA (lower panels). **(I)** Immunoblot analysis of transgenic Arabidopsis lines that express HopE1-HA or one of the HopE1 CaM-binding site mutants HopE1_{F178A}, HopE1_{L182A}, and HopE1_{F184A}. Samples were subjected to immunoblot analysis with anti-HA antibodies. **(J-K)** Experiments used Arabidopsis plants that express HopE1-HA, HopE1_{F178A}, HopE1_{L182A}, or HopE1_{F184A} treated with 1 μM flg22. **(J)** Callose deposition in Arabidopsis plants that express HopE1-HA or one of the HopE1-HA CaM-binding site mutants. **(K)** ROS production in Arabidopsis plants that express HopE1-HA or one of the HopE1-HA CaM-binding site mutants. RLU, relative luminescence unit, n=24.

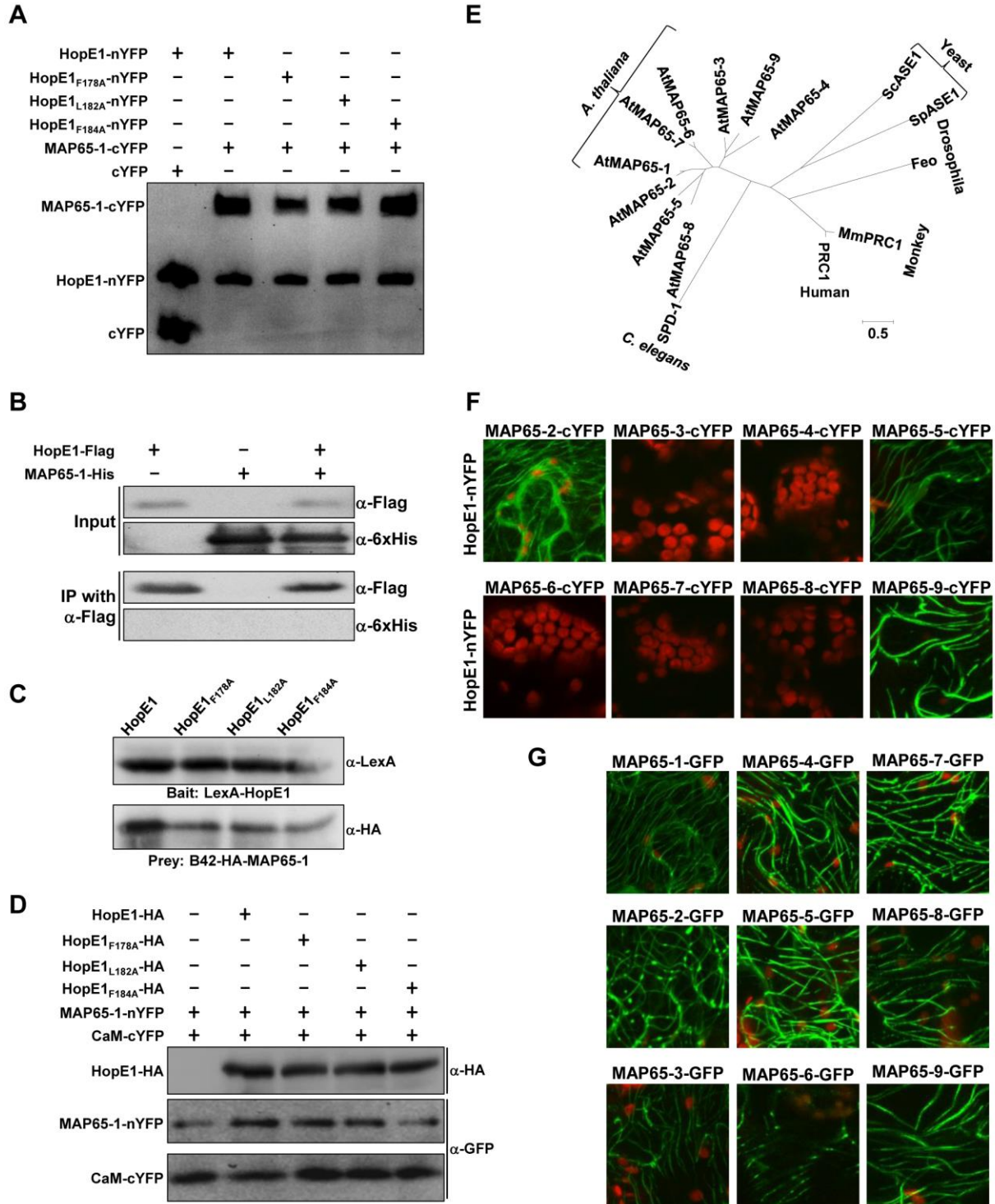


Figure S3. HopE1 can Interact with a Subset of MAP65 Family Members, Related to Figure 3. (A)

Immunoblots showing expression of proteins used in BiFC assay in Fig. 3A. **(B)** Bacterially-expressed HopE1 and MAP65-1 do not interact with each other. Crude extracts from an *E. coli* culture expressing HopE1-Flag and MAP65-1-His were used in pull-down assays using anti-Flag resin. **(C)** Immunoblots showing expression of MAP65-1 and HopE1 derivatives in yeast strains used in Fig. 3C. **(D)** Immunoblots showing expression of proteins

used in BiFC assay in Fig. 3D. **(E)** A phylogenetic tree showing different clades of the MAP65/Ase1/PRC1 family. **(F)** HopE1 interacts with a subset of MAP65 family members in BiFC assays. All nine MAP65 homologs from Arabidopsis were cloned into the binary vector pLN462, which results in each being fused with cYFP. These were co-expressed with HopE1-nYFP in *N. benthamiana* using agroinfiltrations. **(G)** Localization of Arabidopsis MAP65 family proteins in plant cells using C-terminal GFP fusions.

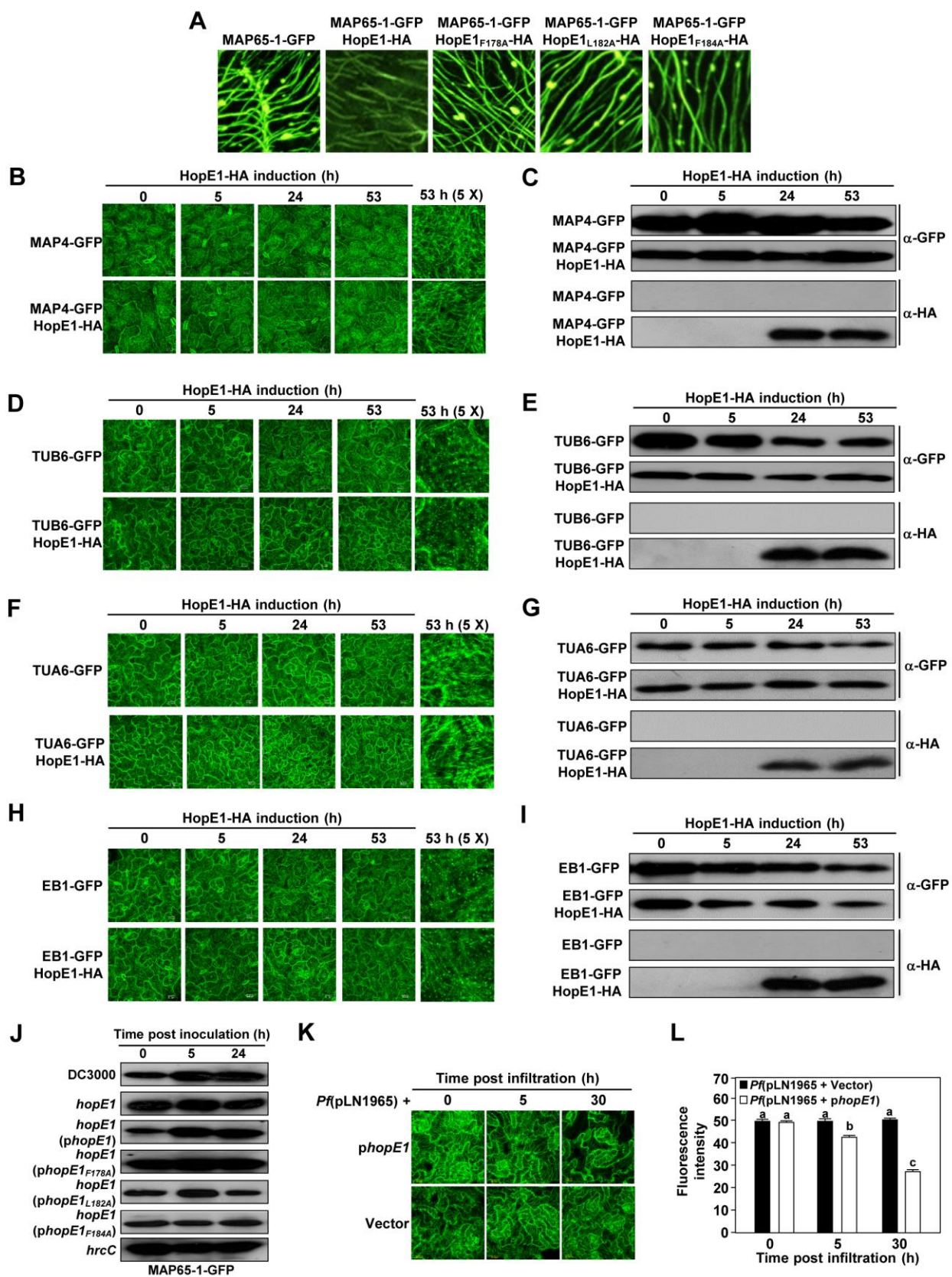


Figure S4. HopE1 Dissociates MAP65-1-GFP from Microtubules, but not MAP4-GFP, TUB6-GFP, TUA6-GFP, or EB1-GFP, Related to Figure 4. (A) 25X magnification of the micrographs from Fig. 4A (at 50 hour time point). (B, D, F, & H) Arabidopsis transgenic plants expressing a microtubule-related GFP fusion protein only or with HopE1-HA were treated with estradiol to induce HopE1-HA production and GFP fluorescence was monitored with confocal microscopy at the indicated times (hours). (C, E, G, & I) Crude extracts were prepared from Arabidopsis tissues at the indicated time points (hours) after estradiol treatment and used in immunoblots with anti-GFP and anti-HA antibodies. (B) MAP4-GFP fluorescence with or without HopE1. (C) Immunoblot analysis of MAP4-GFP and HopE1-HA. (D) TUB6-GFP fluorescence with or without HopE1. (E) Immunoblot analysis of TUB6-GFP and HopE1-HA. (F) TUA6-GFP fluorescence with or without HopE1. (G) Immunoblot analysis of TUA6-GFP and HopE1-HA. (H) EB1-GFP fluorescence with or without HopE1. (I) Immunoblot analysis of EB1-GFP and HopE1-HA. (J) Immunoblot analysis of samples from transgenic Arabidopsis plants expressing MAP65-1-GFP infiltrated with *Pto* DC3000, *Pto* DC3000 *hopE1* mutant, *hopE1*(*phopE1*), *hopE1*(*phopE1*_{F178A}), *hopE1*(*phopE1*_{L182A}), *hopE1*(*phopE1*_{F184A}), or the type III-defective *hrcC* mutant. These samples were from the leaf tissue used for the micrographs shown in Fig. 4D. (K) Arabidopsis MAP65-1-GFP transgenic plants were syringe-infiltrated with *P. fluorescens*(pLN1965) with or without *phopE1* at 10⁷ cells/ml. This strain produces a functional type III system and injects HopE1 into plant cells. MAP65-1-GFP was monitored with confocal microscopy at the indicated time points (in hours) after infiltration. (L) Quantification of MAP65-GFP fluorescent signal in the plants used in panel (K). Different lowercase letters indicate statistical significance between time points (P<0.05). The values are means ± SEM, n=30.

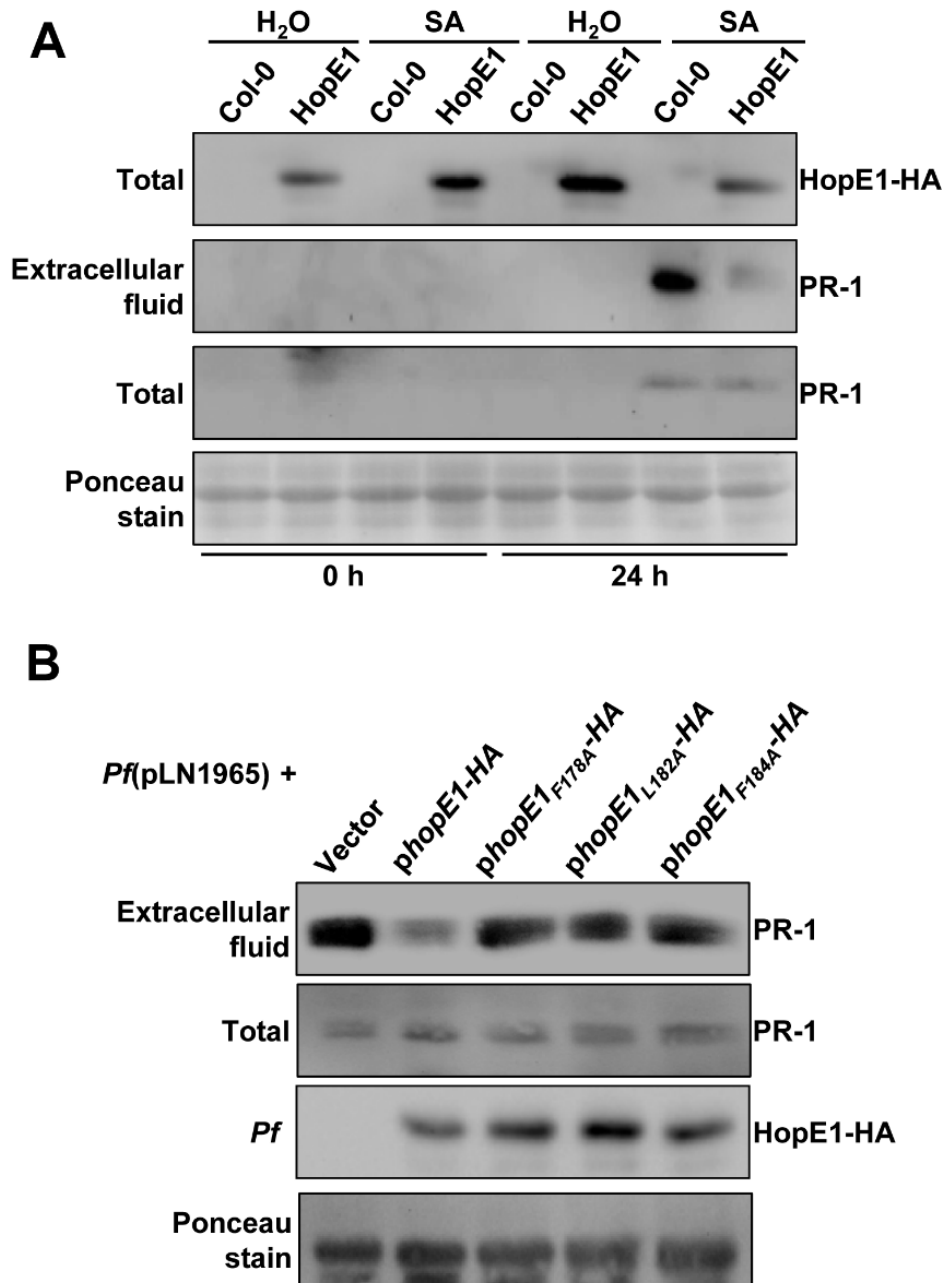


Figure S5. PR-1 Secretion is Inhibited by HopE1, Related to Figure 5. (A) Arabidopsis Col-0 and transgenic Arabidopsis expressing HopE1-HA were treated with estradiol. After 24 hours, the plants were treated with SA (200 μ M) or H₂O as a mock control. (B) PR-1 secretion is inhibited by bacterially delivered HopE1. Arabidopsis Col-0 was infiltrated with *P. fluorescens*(pLN1965) strains carrying pML123, *phopE1*, *phopE1*_{F178A}, *phopE1*_{L182A}, *phopE1*_{F184A}. (A & B), Leaves were vacuum-infiltrated with PBS (pH 7.4) at the time of infiltration and/or after 24 hours. Extracellular fluids were collected from vacuum-infiltrated leaves by centrifugation. Anti-HA and anti-PR-1 antibodies were used to detect HopE1-HA and PR-1, respectively. A Ponceau S stain of the membrane is shown to evaluate the relative protein levels of the samples.

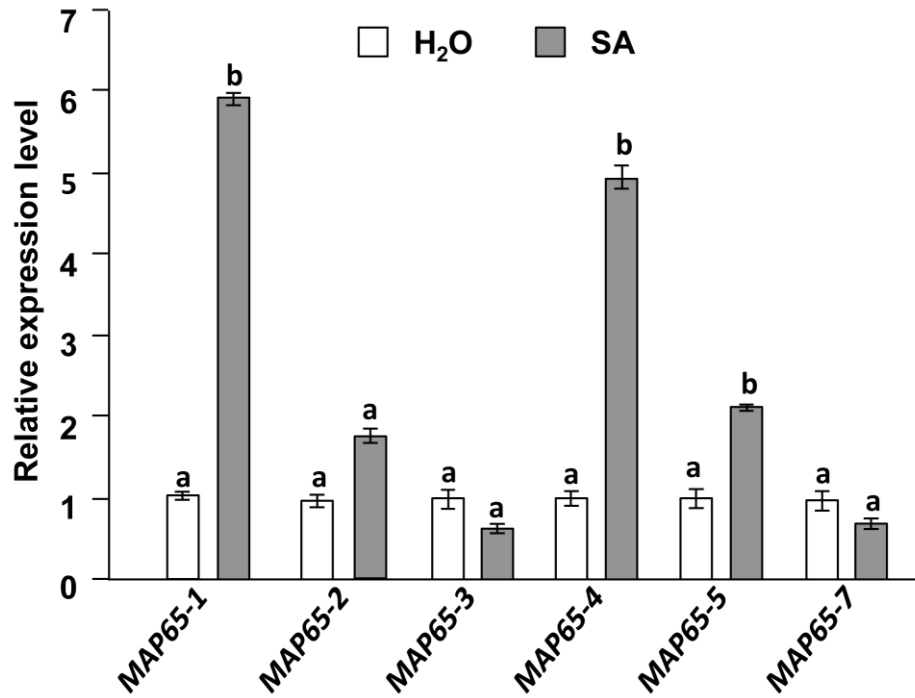


Figure S6. Additional evidence that MAP65-1 is a component of plant immunity, Related to Figure 6. *MAP65* gene expression as measured by quantitative RT-PCR after salicylic acid (SA) or mock treatments. Statistical significance was analyzed by student t-test ($P < 0.05$). Standard error bars are indicated. Similar results were observed in three independent experiments.

Table S1. HopE1 Interacts with Calmodulins and MAP65-1 in Yeast Two-hybrid Screens, Related to Experimental Procedures

Gene	Annotation
AT5G37780	Calmodulin 1
AT3G56800	Calmodulin 3
AT1G66410	Calmodulin 4
AT2G27030	Calmodulin 5
AT5G21274	Calmodulin 6
AT3G43810	Calmodulin 7
AT5G55230	Microtubule-associated protein 65-1

Table S2. Plasmids and Strains Used in This Study, Related to Experimental Procedures.

Table S3. Primers Used for Cloning and RT-PCR, Related to Experimental Procedures.

Supplemental Experimental Procedures

Construction of *P. syringae* DC3000 *hopE1* Mutants

Upstream and downstream DNA regions from the *hopE1* gene were PCR-amplified with Pfu polymerase (Stratagene), then cloned into the pENTR-D TOPO vector (Invitrogen). The resulting pENTR constructs were recombined with suicidal destination vectors pMK2016 and pMK2017 by LR reactions, respectively. Both pMK2016- and pMK2017-derived constructs were integrated into the *Pto* DC3000 chromosome by homologous recombination by tri-parental or bi-parental mating. The *hopE1* deletion mutants were selected for by screening putative mutants for the loss of both spectinomycin and tetracyclin resistance. The strains containing *hopE1* deletions were then grown on sucrose containing King's B (KB)(King et al., 1954) plates for counter-selection of pHP474.

Plant Materials

Double transgenic plants expressing 35S-MAP65-1-GFP and HopE1-HA, HopE1_{F178A}-HA, HopE1_{L182A}-HA, or HopE1_{F184A}-HA under estradiol inducible promoter were made by crossing individual transgenic lines. All Arabidopsis plants were grown at 24°C with 10 hours of light/day in micro-climate controlled growth chambers. *N. benthamiana* plants were grown in standard greenhouses.

In planta Bacterial Growth Assay

Overnight cultures of *P. syringae* strains grown on KB agar were resuspended to a cell density of 10⁸ cells/ml in 10 mM MgCl₂. Five-week-old Arabidopsis plants were spray-inoculated with bacterial suspensions containing 0.002% Silwet L-77™. Leaf disks of 0.3 cm in diameter were punched with a cork borer at the indicated times after inoculations. The samples were ground in sterile distilled water, and 10-fold serial dilutions were plated on KB agar plates. The bacteria were enumerated after 2-3 days at 30°C.

Callose Deposition Assay and Quantification of Callose

For callose examination, five-week-old Arabidopsis or transgenic plant leaves were infiltrated with flg22 (1 μM), elf18 (1 μM), or 100 μg/ml chitin using a needleless syringe. For callose assay with *P. fluorescens* (*Pf*)(pLN1965) strains, Arabidopsis leaves were infiltrated with *Pf*(pLN1965) strains carrying *phopE1*, *phopE1*_{F178A}, *phopE1*_{L182A}, *phopE1*_{F184A}, and a vector control at 10⁷ cells/ml. The callose deposits were stained with aniline blue and visualized by capturing images with a Zeiss Axioplan 2 microscope. The numbers of callose deposits were quantified using ImageJ (<http://imagej.nih.gov/ij/>). Briefly, the callose image files were opened with ImageJ. The menu Image/Type/8-bit was selected to convert the callose picture into an 8-bit grey picture. Then the Image/Adjust/threshold was selected to adjust threshold to the level that shows red dots close to the proximity of the callose foci in the original color pictures. Next Analyze/Analyze Particles was selected, followed by the selection of the setting criteria Size and Summary. The summarized data were then pasted into an Excel worksheet for further statistical analysis.

Quantification of GFP Fluorescence Intensity

MAP65-1-GFP transgenic plants or transgenic plants expressing both MAP65-1-GFP and HopE1-HA and HopE1 calmodulin (CaM)- binding site mutant derivatives were treated with 20 μM estradiol to induce HopE1-HA. The GFP fluorescence was monitored with confocal microscope by capturing images at indicated time points after induction. The GFP fluorescence intensity was quantified with ImageJ. The fluorescence was quantified from 3 fields of view for each sample. In each, 10 plant cells were used for quantification. Briefly, the GFP images files are open with ImageJ (<http://imagej.nih.gov/ij/>). The menu Image/Split channels is selected if the images contain multiple channels. Then the green channel pictures are selected. The cells of interest are selected using any of the drawing/selection tools (i.e., rectangle, circle, polygon, or freeform). Set Measurements is selected from the Analyze menu. AREA, INTEGRATED DENSITY and MEAN GRAY VALUE are selected from the popup menu. The menu Measure is selected from the Analyze menu. A popup box shows a stack of values for that first cell. The same process is repeated to measure the other cells. All the data in the Results window can be copied and pasted into a new excel worksheet for further statistical analysis.

CaM Affinity Resin Pull-downs

Protein samples were incubated with CaM affinity resin (Agilent Technologies) for 4 hours. Resin samples were washed 3 times with binding buffer to remove unbound proteins. The bound proteins were eluted by washing with

50 mM Tris, 150 mM NaCl, 2 mM EGTA, pH 7.5. For bacterial protein samples, *E. coli* BL21 carrying pLN4420 that expresses HopE1-His was grown in liquid LM with antibiotics until the culture reached an OD₆₀₀ of 0.6 and then was induced with IPTG (1 mM) and grown an additional 3 hours. The cultures were resuspended with binding buffer (50 mM Tris, 150 mM NaCl, 2 mM CaCl₂, pH7.5) or the same buffer containing 2 mM EGTA. Cell suspensions were lysed by sonication and cleared by centrifugation at 10,000 rpm for 20 min. For plant protein samples, *N. benthamiana* leaves were infiltrated with *Agrobacterium* strains carrying plasmids expressing HopE1-HA, MAP65-1-HA, or co-infiltrated with both strains. Transformed leaves were ground in liquid nitrogen and resuspended in binding buffer. The samples were then clarified by centrifugation at 12,000 rpm at 4°C.

***In vitro* CaM-Binding Assay**

The *in vitro* binding of synthetic peptides with CaM was determined using a previously reported gel mobility shift assay with some modification (Arazi et al., 1995; Yang et al., 2010). Briefly, peptides corresponding to the HopE1 or CBP60g CaM-binding sites were synthesized by Sigma. Bovine CaM at 125 nM (Sigma) was incubated with the HopE1 peptide or CBP60g peptide at different molar ratios (0, 1, 1.5, 2, 2.5, and 3.0) in 100 mM Tris-HCl, pH 7.2, and containing either 0.1 mM CaCl₂ or 2 mM EGTA in a total volume of 40 µl at room temperature for 1h. The mixtures were subjected to a 4-15% gradient native PAGE (Bio-Rad) followed by standard Coomassie blue staining.

Supplemental References

- Arazi, T., Baum, G., Snedden, W.A., Shelp, B.J., and Fromm, H. (1995). Molecular and biochemical analysis of calmodulin interactions with the calmodulin-binding domain of plant glutamate decarboxylase. *Plant Physiol* 108, 551-561.
- Choi, K.H., Gaynor, J.B., White, K.G., Lopez, C., Bosio, C.M., Karkhoff-Schweizer, R.R., and Schweizer, H.P. (2005). A Tn7-based broad-range bacterial cloning and expression system. *Nat Methods* 2, 443-448.
- Crabill, E., Karpisek, A., and Alfano, J.R. (2012). The *Pseudomonas syringae* HrpJ protein controls the secretion of type III translocator proteins and has a virulence role inside plant cells. *Molecular microbiology*, no-no.
- Cuppels, D.A. (1986). Generation and characterization of Tn5 insertion mutations in *Pseudomonas syringae* pv. *tomato*. *Appl Environ Microbiol* 51, 323-327.
- Guo, M., Tian, F., Wamboldt, Y., and Alfano, J.R. (2009). The majority of the type III effector inventory of *Pseudomonas syringae* pv. *tomato* DC3000 can suppress plant immunity. *Mol Plant Microbe Interact* 22, 1069-1080.
- Gyuris, J., Golemis, E., Chertkov, H., and Brent, R. (1993). Cdk1, a human G1 and S phase protein phosphatase that associates with Cdk2. *Cell* 75, 791-803.
- Hanahan, D. (1983). Studies on transformation of *Escherichia coli* with plasmids. *J Mol Biol* 166, 557- 580.
- House, B.L., Mortimer, M.W., and Kahn, M.L. (2004). New recombination methods for *Sinorhizobium meliloti* genetics. *Appl Environ Microbiol* 70, 2806-2815.
- Jamir, Y., Guo, M., Oh, H.-S., Petnicki-Ocwieja, T., Chen, S., Tang, X., Dickman, M.B., Collmer, A., and Alfano, J.R. (2004). Identification of *Pseudomonas syringae* type III effectors that suppress programmed cell death in plants and yeast. *Plant J* 37, 554-565.
- Karimi, M., Inze, D., and Depicker, A. (2002). GATEWAY vectors for *Agrobacterium*-mediated plant transformation. *Trends Plant Sci* 7, 193-195.
- King, E.O., Ward, M.K., and Raney, D.E. (1954). Two simple media for the demonstration of pyocyanin and fluorescein. *J Lab Clin Med* 44, 301-307.
- Labes, M., Puhler, A., and Simon, R. (1990). A new family of RSF1010-derived expression and *lac*-fusion broad-host-range vectors for gram-negative bacteria. *Gene* 89, 37-46.
- Ruvkin, G.B., and Ausubel, F.M. (1981). A general method for site-directed mutagenesis in prokaryotes. *Nature* 289, 85-88.
- Yang, L., Ji, W., Zhu, Y., Gao, P., Li, Y., Cai, H., Bai, X., and Guo, D. (2010). GsCBRLK, a calcium/calmodulin-binding receptor-like kinase, is a positive regulator of plant tolerance to salt and ABA stress. *J Exp Bot* 61, 2519-2533.
- Zuo, J., Niu, Q., and Chua, N. (2000). An estrogen receptor-based transactivator XVE mediates highly inducible gene expression in transgenic plants. *Plant J* 24, 265-273.